Pozitivan učinak C-terminalnog rigidnog linkera na imobilizaciju saharoze fosforilaze

Mikac, Ivan

Master's thesis / Diplomski rad

2022

Degree Grantor / Ustanova koja je dodijelila akademski / stručni stupanj: **University of Zagreb, Faculty of Food Technology and Biotechnology / Sveučilište u Zagrebu, Prehrambeno-biotehnološki fakultet**

Permanent link / Trajna poveznica: https://urn.nsk.hr/urn:nbn:hr:159:812823

UNIVERSITY OF ZAGREB
FACULTY OF FOOD TECHNOLOGY AND BIOTECHNOLOGY

GRADUATE THESIS

Zagreb, September 2022

Ivan Mikac

POSITIVE EFFECT OF C-TERMINAL RIGID LINKER ON IMMOBILIZATION OF SUCROSE PHOSPHORYLASE

This study was carried out at the Institute of Biotechnology and Biochemical Engineering of the Faculty of Technical Chemistry, Chemical and Process Engineering and Biotechnology at the Graz University of Technology under the supervision of Bernd Nidetzky, Univ.-Prof. Dipl.-Ing. Dr. techn., with the assistance of Chao Zhong, Dr. Eng., and Prof. dr. sc. Anita Slavica, Faculty of Food Technology and Biotechnology University of Zagreb,

This Graduate Thesis was a part of HOTZYMES: The Development of efficient Enzymatic Cascades in well-coordinated One-Pot-Systems, funded by the European Union (EU) and coordinated by Prof. dr. sc. Valeria Grazú. The consortium consists of 7 partners (including TU Graz) from 4 European countries.

ACKNOWLEDGMENTS

I would like to thank my supervisor, Univ. Prof. Dipl. Ing. Dr. techn. Bernd Nidetzky, for the opportunity to conduct my graduate thesis at the Institute of Biotechnology and Biochemical Engineering at the Graz University of Technology, as part of his research group.

I would also like to thank Chao Zhong, Dr. Eng. for his advice, help, and guidance during my stay in Graz and during my Thesis writing, pushing me to be the best version of myself. In addition, I would like to thank MSc Anisha Vyas for showing me several techniques during my stay in Graz and the whole BIOTE team for their cooperation and creation of a comfortable work environment.

Many thanks to Prof. dr. sc. Anita Slavica for the given opportunity, effort, and time invested in my Graduate Thesis.

A big thanks to my family, girlfriend, and friends for their constant support, unconditional love, and motivation during my whole educational journey.

BASIC DOCUMENTATION CARD

Graduate Thesis

University of Zagreb
Faculty of Food Technology and Biotechnology
Department of Biochemical Engineering
Laboratory for Biochemical Engineering, Industrial Microbiology and Malting and Brewing Technology
Scientific area: Biotechnical Sciences
Scientific field: Biotechnology

Positive effect of C-terminal rigid linker on immobilization of a sucrose phosphorylase

Ivan Mikac, univ. bacc. ing. techn. aliment.
0058210684

Abstract: Gene coding for sucrose phosphorylase (SP) from *Leuconostoc mesenteroides* (*Lm*) was inserted into pET21b with N- (N, His_6-*Lm*SP) or C-terminal (C) His_6-tag (*Lm*SP-His_6) and rigid linker (L) consisted of repetitive sequences of $(EAAAK)_n$ with n = 6 (~5 nm) and 14 (~10 nm) or n = 6 (~5 nm), 14 (~10 nm) and 19 (~15 nm), respectively. Fused genes and the plasmid were used for electroporation of *E. coli* (BL21)DE3 and constructs were expressed, isolated, and purified by affinity chromatography. Since inclusion bodies were observed with N-terminally fused linkers, only C-terminally His_6-tagged constructs with higher specific activity were considered for immobilization experiments. The immobilization of the control and *Lm*SP-CL_{5nm} on SEPABEADS^{TM} EC-EP was successful without any unbound protein in the supernatant. Due to its size, the rigid linker of *Lm*SP-CL_{15nm} completely prevented Cu^{2+}(SEPABEADS^{TM} EC-EP) and His_6 (the construct) coupling. The control and three *Lm*SP-CL constructs were readily bound to Ni-NTA Superflow and had a higher immobilization yield than the control, with the highest immobilization efficiency of *Lm*SP-CL_{15nm}.

Keywords: *Leuconostoc mesenteroides* sucrose phosphorylase (*Lm*SP), rigid linkers, enzyme immobilization.
Thesis contains: 56 pages, 19 figures, 20 tables, 63 references, 0 supplements
Original in: English
Graduate Thesis in printed and electronic (pdf format**) form is deposited in:** The Library of the Faculty of Food Technology and Biotechnology, University of Zagreb, Kačićeva 23, Zagreb.
Mentor: Anita Slavica, PhD, Full Professor
Co-mentor: Bernd Nidetzky; Univ.-Prof. Dipl.-Ing. Dr. techn.
Technical support and assistance: Chao, Zhong, Dr. Eng.

Reviewers:
1. Renata Teparić, PhD, Full professor
2. Anita Slavica, PhD, Full professor
3. Bernd Nidetzky, Univ.-Prof. Dipl.-Ing. Dr. techn., Full professor
4. Blaženka Kos, PhD, Full professor

Thesis defended: 30th of September 2022

TEMELJNA DOKUMENTACIJSKA KARTICA

Diplomski rad

Sveučilište u Zagrebu
Prehrambeno-biotehnološki fakultet
Zavod za biokemijsko inženjerstvo
Laboratorij za biokemijsko inženjerstvo, industrijsku mikrobiologiju i tehnologiju piva i slada
Znanstveno područje: Biotehničke znanosti
Znanstveno polje: Biotehnologija

Pozitivan učinak C-terminalnog rigidnog linkera na imobilizaciju saharoze fosforilaze

Ivan Mikac, univ. bacc. ing. techn. aliment.
0058210684

Sažetak: Gen koji kodira saharozu fosforilazu (SF) iz *Leuconostoc mesenteroides* (*Lm*) je insertiran u pET21b sa N- (N, His_6-*Lm*SF) ili C-terminalnim (C) His_6-tag-om (*Lm*SF-His_6) i rigidnim linkerom (L), koji je načinjen od ponavljajućih sekvenci $(EAAAK)_n$, gdje je, redom, n = 6 (~5 nm) i 14 (~10 nm) ili n = 6 (~5 nm), 14 (~10 nm) i 19 (~15 nm). Geni fuzirani u plazmid korišteni su za elektroporaciju *E. coli* (BL21)DE3 i ovi konstrukti su eksprimirani, izolirani i pročišćeni afinitetnom kromatografijom. Inkluzijska tijela su formirana kod linkera na N-kraju proteina, pa su samo konstrukti sa His_6-tag-om na C-kraju proteina sa višom specifičnom aktivnosti korišteni u eksperimentima imobilizacije. Imobilizacija kontrole i *Lm*SP-CL_{5nm} na nosaču SEPABEADS^{TM} EC-EP bila je uspješna, te nevezani proteini nisu detektirani u supernatantu. Zbog svoje veličine, rigidni linker u *Lm*SP-CL_{15nm} potpuno je spriječio povezivanje Cu^{2+}(SEPABEADS^{TM} EC-EP) i His_6 (s konstrukta). Kontrola i tri konstrukta *Lm*SP-CL direktno su se vezali na Ni-NTA Superflow i, u usporedbi s kontrolom, uspješnija je bila imobilizacija ovih konstrukata, a najveća imobilizacijska učinkovitost je procijenjena kod *Lm*SP-CL_{15nm}.

Ključne riječi: Saharoza fosforilaza iz *Leuconostoc mesenteroides* (*Lm*SP), rigidni linkeri, imobilizacija enzima.
Rad sadrži: 56 stranica, 19 slika, 20 tablica, 63 literaturna navoda, 0 priloga
Jezik izvornika: engleski
Rad je u tiskanom i elektroničkom (pdf format) obliku pohranjen u: Knjižnica Prehrambeno-biotehnološkog fakulteta, Kačićeva 23, Zagreb
Mentor: Prof. dr. sc. Anita Slavica
Komentor: Univ.-Prof. Dipl.-Ing. Dr. techn. Bernd Nidetzky, Institute of Biotechnology and Biochemical Engineering, TU Graz
Pomoć pri izradi: Chao Zhong, Dr.Eng.

Stručno povjerenstvo za ocjenu i obranu:

1. Prof. dr. sc. Renata Teparić
2. Prof. dr. sc. Anita Slavica
3. Univ. Prof. Dipl. Ing. Dr. techn. Bernd Nidetzky
4. Prof. dr. sc. Blaženka Kos

Datum obrane: 30. rujan 2022

1. INTRODUCTION

Sugarcane is the primarily grown crop for sugar production, supplying 86 % of the world's sugar requirements (the remaining from sugar beet). It is generally grown in tropical countries and serves both as a food and fuel source (as sugarcane ethanol), with the food manufacturing sector consuming 75 % of the produced sugarcane, while the balance is used in biofuel production. Cane sugar, obtained from processing sugarcane, had in 2017 an export value of 24.7 billion USD, with the largest cane sugar exporting countries being Brazil (11.4 billion USD), Thailand (2.6 billion USD), and France (1.3 billion USD). The largest cane sugar importing countries were Indonesia (2.3 billion USD), the United States (1.7 billion USD), and Bangladesh (1.1 billion USD) (Voora et al., 2020). Sugar consumption *per capita* in the world was rising for several decades, but came to a stop when associated with obesity, which may result in adverse metabolic, biomechanical, and psychosocial health consequences (Faruque et al., 2019). In this light, the World Health Organisation strongly recommends lowering the dietary intake of sugars and pressuring multi-billion-dollar companies to reduce sugar in their products. As a result, several organizations [the Organization for Economic Co-operation and Development (OECD), and the Food and Agriculture Organization of the United Nations (FAO)] predict the lowering of sugarcane production from 2.1 % to 1.1 % annually from 2018 to 2027. Growth of cane sugar already outpaced the demand growth for human consumption from 2016 to 2017, at a rate of 8 % in comparison to the expected 2 % and resulted in a global cane sugar excess of approximately 11 million tonnes. As planted areas in Asia (specifically China and Indonesia) expand and farm productivity improves, the surplus is expected to persist, according to projections through the year 2025 (Voora et al., 2020). The demand for sucrose is lowering and the problems of oversupply begin to emerge. Solutions to these problems had to be found, and an innovative alternative for the use of sucrose are trans-glycosylation technologies, which convert sucrose into a wide range of valuable products. In most cases, these products (rare sugars, vitamins, flavours, antibiotics, fragrances, glycosides, *etc*.) have health-promoting properties. A promising enzyme in this aspect is sucrose phosphorylase (SP) (EC 2.4.1.7), which catalyses the reversible phosphorolysis of sucrose with inorganic phosphate (Pi) into α-D-glucose 1-phosphate (Glc1-P) and fructose (Franceus and Desmet, 2020). This enzyme is classified as a glycosyl transferase, precisely a hexosyltransferase, although it is part of the glycoside hydrolase family (GH13). It is generally found in *Bifidobacterium* and lactic acid bacteria, where it partakes in energy metabolism reactions (Cerdobbel et al., 2010a). This

enzyme contains about 500 amino acids and was found to occur as a functional monomer or dimer and does not require cofactors and co-substrates (Goedl et al., 2010). The chemical industry represents one of the biggest economic sectors worldwide and enzymes, including SP, play a crucial role in new technologies introduced to well-established manufacturing processes (Schmid et al., 2002). Industrial applications of enzymes are often hindered by the lack of long-term operational stability and being difficult to recover (Sheldon, 2007), which are specifically intractable for the enzymes that catalyse carbohydrate conversion, ideally performing at above 60 °C to avoid contaminations. SP has been isolated from a series of microorganisms such as *Bifidobacterium adolescentis* (van den Broek et al., 2004)*, Pseudomonas saccharophila* (Weimberg and Doudoroff, 1954)*, Streptococcus mutans* (Russell et al., 1988) and *Leuconostoc mesenteroides* (Goedl et al., 2007), however, none of them are thermophilic. The only exception is the SP isolated from *B. adolescentis,* which functions optimally at pH 6.5 and 58 °C (Cerdobbel et al., 2010a). Therefore, the thermo-instability of SP is a crucial limitation for its industrial utilization. To overcome this, enzyme immobilization could be a promising solution (Hermanová et al., 2015; Guzik et al., 2014; Hsieh et al., 2000). Indeed, Cerdobbel et al. (2010b) have shown that the thermostability of SP is improved through immobilization *via* covalent coupling to SEPABEADS^{TM} EC-HFA (amino-epoxy activated) carriers or through cross-linked enzyme aggregates. In most cases, however, enzyme activity is permanently lost during immobilization due to unwanted interactions between enzymes and carriers, resulting in conformational changes and difficulties in substrate-enzyme interactions. The goal of this study was to determine the effect of rigid linkers insertion on the N- and C-terminus of SP and their length on the perseverance of activity during immobilization. In the current study, the fusion of rigid linkers [*i.e.* $(EAAAK)_n$, n varied from 6-19, linker length in the range of approximately 5-20 nm] to sucrose phosphorylase from *Leuconostoc mesenteroides* (*Lm*SP) (either N- or C-terminus) was achieved through prolonged overlap extension-PCR (POE-PCR) (Zhong et al., 2017), and these fusion complexes were expressed in *E. coli* (BL21)DE3 and characterized. The immobilization of these complexes on two different carriers (SEPABEADS^{TM} EC-EP and Ni-NTA Superflow) was carried out to determine the effect of the linker and its lengths on the immobilization of *Lm*SP. Overall, this study could provide a better understanding of the effect of interspace or interfacial interaction on enzyme immobilization.

2. LITERATURE REVIEW

2.1. Enzymes

Enzymes are defined as biological macromolecules containing one or more polypeptide chains, which can increase the rate of a biochemical reaction without changing the reaction equilibrium and not being permanently altered or consumed by the reaction (Zucca et al., 2016). They are found in living cells, where they have the function of natural biocatalysts and enhance the rate of almost all chemical reactions. The reaction rates are speeded up 10^6 – 10^7-fold, so reactions which take years to spontaneously complete can occur within fractions of a second when the appropriate enzyme is present.

In this case, the presence of enzymes lowers the activation energy, which results in less energy needed to complete a chemical reaction. Enzymes have a complex three-dimensional structure, forming active sites in which the enzyme and substrate(s) interact. Therefore, the enzyme and its substrate(s) bind tightly together and form an enzyme-substrate complex. The binding brings key atoms in approach to each other and stresses key covalent bonds, which results in a chemical reaction (Berg et al., 2013). For enzyme kinetics, two key parameters, *i.e.* the K_m and the v_{max}, are normally considered. v_{max} is defined as the velocity of the catalysed biochemical/chemical reaction that would be obtained if the enzyme is fully saturated with its substrate. K_m (Michaelis constant) corresponds to dissociation constant of the enzyme-substrate complex, and represents a measure of the substrate affinity of the enzyme. K_m represents the substrate concentration at which the reaction velocity has a value half of v_{max}, or, in other words, when half of the enzyme active sites are saturated. Their relation can be seen in the equation below, which was designed by Leonor Michaelis and Maud Leonora Menten:

$$v = \frac{v_{max}\,[S]}{K_m + [S]} \qquad [1]$$

where v is the reaction velocity (amount of product formed in a certain period), v_{max} is the maximum reaction velocity, [S] is the substrate concentration, K_m is the concentration of the substrate at $v_{max}/2$.

Enzymes are efficient catalysts that operate under mild conditions (ambient temperature and pressure, physiological pH, aqueous environment), which all have an economical value and decrease the cost of an industrial process. In addition, biocatalysts perform precise reactions due to their excellent regio-, chemo-, or stereo-specificity and selectivity (Zucca et al., 2016).

Despite the advantages of enzymes, their use is sometimes associated with drawbacks such as sensitivity to process conditions, low stability, and possible inhibition by high concentrations of reaction components (Garcia-Galan et al., 2011; Schoemaker et al., 2003). Therefore, the use of enzymes in industrial applications is difficult. Different strategies have been investigated to make enzymes more favourable for applications, including enzyme immobilization (Mohamad et al., 2015)

2.1.1. Sucrose phosphorylase (SP)

SP (EC 2.4.1.7) is a promising enzyme in transglycosylation technologies, wherein rare sugars with health-promoting properties and glycosides of small molecules such as flavours, antibiotics, fragrances, and vitamins are produced. In living systems, this enzyme catalyses the reversible phosphorolysis of sucrose in the presence of Pi, generating Glc-1-P and fructose (Goedl et al., 2007). The reaction mechanism can be explained as a double displacement mechanism where a carboxylic residue attacks the anomeric carbon of sucrose, generating a covalent β-glucosyl-enzyme intermediate. This intermediate can step into a reaction with phosphate (phosphorolysis), water (irreversible hydrolysis), and external nucleophiles (transglycosylation), giving different products (Figure 1.) (Franceus and Desmet, 2020).

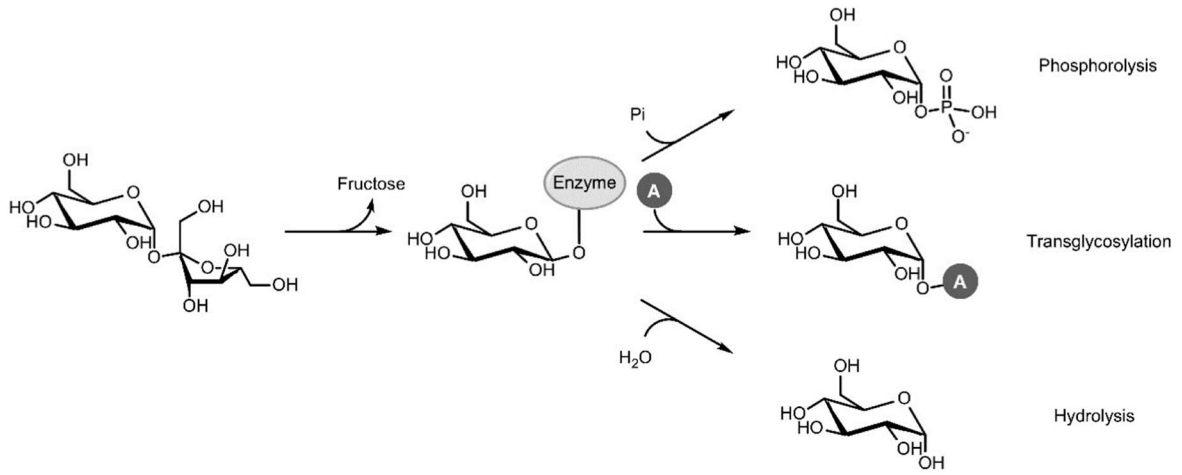

Figure 1. Scheme of reactions catalyzed by SP. The β-glucosyl-enzyme intermediate and fructose are generated after a carboxylic residue attacks the anomeric carbon of sucrose. Depending on the reactant, phosphorolysis (Pi), transglycosylation (nucleophile), or hydrolysis (H_2O) occurs, where Pi is inorganic phosphate, and A is an acceptor/nucleophile (Franceus and Desmet, 2020)

This enzyme has been isolated from several bacterial strains and served as an early model enzyme. It was used to examine and understand the mechanism of enzymatic glycosyl transfer. Goedl et al. (2007) previously described the kinetic parameters and properties of recombinant SP (containing an 11 amino-acid long N-terminal metal affinity fusion peptide) from *L. mesenteroides*. The maximum initial rate of phosphorolysis and synthesis were 180 and 105 $U/mg_{enzyme,}$ respectively, where the K_m values were similar for phosphate (9.5 ± 0.7 mM, determined at 250 mM sucrose) and sucrose (5.7 ± 0.3 mM, determined at 50 mM phosphate), D-fructose (21.2 ± 3.7 mM, determined at 100 mM Glc-1-P) and Glc-1-P (17.3 ± 1.1 mM, determined at 100 mM D-fructose). The optimum pH for both directions of the reaction was 6.5-7.0, where the binding strength of sucrose was four times tighter than that of D-fructose. It was also suggested that glycosylation from sucrose occurs more efficiently than Glc-1-P. The obtained kinetic parameters for the His-tagged and native *Lm*SP were similar and comparable. In addition, the stability of the recombinant *Lm*SP was highest in the pH of 7.0-7.5, however at a temperature below 30 °C (Table 1.).

Table 1. Stability of recombinant *Lm*SP: (a) at 30 °C after 100 h with varying pH; (b) at pH 7.0 after 100 h with varying temperatures (Goedl et al., 2007)

a)

pH	log (activity)
5.5	0.6
6.0	0.7
6.5	1.4
7.0	1.8
7.5	1.8

b)

Temperature (°C)	log (activity)
22	2
30	1.8
40	0
45	0

*Lm*SP is thermosensitive, as shown in Table 1, with its activity well retained only below 30 °C. To extend its application to industrial production where higher temperatures (*e.g.* above 50 °C) are preferable, immobilization of SP is considered a promising solution. Pimentel and Ferreira (1991) immobilized *Lm*SP on DEAE-cellulose while retaining only 18 % of specific activity. During the six days of use, the immobilized enzyme lost 40 % its activity. As compared with the results from Goedl et al. (2007), where recombinant *Lm*SP was immobilized on Eupergit C, showing good stability of immobilized *Lm*SP for the continuous production of Glc1-P up to 650 h, it's suggested that fusion with a peptide (*e.g.* 11 amino-acid N-terminal metal affinity peptide) might improve the stability, activity, and reusability of the immobilized enzyme.

2.2. Enzyme immobilization

Immobilization can be defined as a technical process in which enzymes are fixed on or within solid supports. With this, a heterogeneous immobilized enzyme system is created which shows many advantages, for example, enhanced stability (under both storage and operational conditions), efficient recovery and re-use of enzymes, improved performance, minimal protein contamination of the product, *etc*. (Sheldon, 2007) in comparison to free enzyme systems. These advantages are the result of mimicking natural enzyme environments, where most of them could be attached to organelle structures, the cellular cytoskeleton, or the cellular membrane. Enzymes in such solid support systems generally have a more stable structure than the free enzymes, making them more protected and thus more resistant to environmental changes and allowing them to be re-used. According to Almeida et al. (2022), immobilized biocatalysts can be re-used up to 15 cycles with less than 50 % loss of the initial activity. Sirisha et al. (2016) reported several immobilized enzymes retaining up to 94 % of activity after 12 to 21 cycles of usage. In addition, immobilized enzyme systems show a variety of other advantages, such as rapid termination of reactions, easy recovery of catalysts and products, flexibility in bioreactor designs, application in continuous enzymatic processes, *etc*. However, immobilization generally alters the catalytic properties of the enzymes. One possible explanation is the enhanced restriction of enzymes in accessing their substrates (Homaei et al., 2013). Cerdobbel et al. (2010a) previously characterized the SP from *B. adolescentis* before and after multipoint immobilization. The reported K_m of free and immobilized SP was 6.8 ± 1.2 mM and 9.4 ± 1.3 mM, respectively. Madoery and Fidelio (2001) also immobilized phospholipase A_2 (PLA_2) isolated from cobra venom onto Eupergit C. The immobilized enzyme showed superb stability and reusability. Immobilization, however, altered the kinetic parameters, mainly the v_{max} [v_{max} (free enzyme) = 649 µmol/mg min, v_{max} (immobilized enzyme) = 333 µmol/mg min], whereas the K_m value did not change ($K_m \approx 11.5$ for both free and immobilized enzyme). Similar results were obtained by Knezevic et al. (2006), where the lipase from *Candida rugosa* showed different kinetic parameters before and after immobilization. The obtained K_m value for the free enzyme was 88.5 mmol/L, and the v_{max} was 1.64 µmol/mg min. After immobilization, the K_m value was slightly higher (94.6 mmol/L), but the v_{max} decreased approximately 3-fold (0.51 µmol/mg min).

As it is described by Almeida et al. (2022), in most cases, immobilization directly negatively affects v_{max} and enzyme-substrate affinity, leading to higher K_m. The decreased affinity between the enzyme and substrates probably occurs due to 1) structural (conformational) changes in

enzymes or diffusional limitations of the substrate; and 2) the creation of the Nernst diffusion layer. This phenomenon is described as a layer of solvent around immobilized enzymes, which creates a concentration gradient of the substrate. Methods used in enzyme immobilization can be classified into two groups based on the reversibility of the process: 1) reversible methods, forming weaker bonds, such as hydrogen bonds, affinity binding, van der Waals forces, and ionic binding, between the enzyme and the carriers; and 2) irreversible methods, forming strong covalent bonds (*e.g.* ether, amide, thioether, and carbamate bonds) in between (Almeida et al., 2022).

In addition, according to Nguyen and Kim (2017), immobilization can be classified into various approaches: 1) Adsorption; 2) Covalent binding; 3) Entrapment; and 4) Cross-linking (Figure 2.).

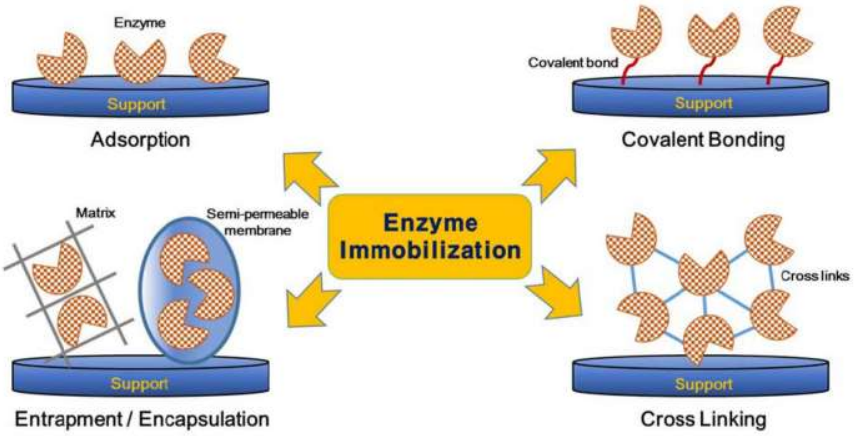

Figure 2. Classification of enzyme immobilization; adsorption: weak enzyme – support binding through Van der Waal's forces or similar weak interactions; covalent bonding: enzyme – support binding through chemical bonds *via* functional groups; entrapment/encapsulation: trapping enzyme molecules inside a polymer matrix; and cross-linking: enzyme cluster creation with intermolecular covalent bonds using a multifunctional reagent (Nguyen and Kim, 2017)

1) Adsorption

Adsorption is considered one of the easiest and most straightforward methods of immobilization, where the enzymes are bound to the carrier with weak bonds such as Van der Waal's forces, hydrophobic and electrostatic interactions. The enzyme solution is mixed with the carriers for a fixed period under conditions where the enzyme activity is preserved. Afterward, the unbound enzyme molecules are washed away with the buffer system. As this method does not involve carrier functionalization and reagent use, it is considered low-cost and non-destructive towards biocatalysts. On the contrary, weak bonds are easily broken as

temperature, pH, or ionic strength changes. Adsorption immobilization is generally divided into 3 sub-categories: physical adsorption, electrostatic binding, and hydrophobic adsorption (Nguyen and Kim, 2017).

2) Covalent bonding

Immobilization through covalent bonding is one of the most commonly used methods, wherein stable enzyme-carrier complexes are formed with strong chemical bonds. It is required that the enzyme contains functional groups, that are non-essential for activity, with which covalent bonds can be made. This occurs through two stages: 1) activation of the carrier surface using multifunctional reagents (linker molecules) such as glutaraldehyde and carbodiimide; and 2) covalent binding of enzyme molecules on the activated carrier. In comparison to adsorption, the incubation time is relatively shorter (*e.g.* several hours) *via* covalent bonding. As strong bonds are formed, a low concentration of enzymes is left unbound during the process, and the enzyme control is better in comparison to adsorption. However, the drawbacks of this method are the high risk of enzyme denaturation (functional groups introduction through chemical modifications), the use of reagents, and the low immobilization yield (Nguyen and Kim, 2017).

3) Entrapment

During entrapment/encapsulation, biocatalysts are trapped within a polymeric matrix, which only permits the diffusion of substrates and products. It involves two steps: 1) creating an enzyme-monomer solution, and 2) polymerization (*via* a chemical reaction or changes in reaction conditions). The enzyme does not interact with the polymers, and therefore no denaturation and loss of activity occurs. In addition, the microenvironment can be adjusted (pH or polarity of the encapsulating material) for the sake of enzyme stability. On the other hand, if the polymerization reaction is extended, the matrix can become condensed and the substrate diffusion would be hindered. Furthermore, if the pore size of the matrix is larger than the enzyme, the leaking of enzyme molecules would occur. There are various methods for encapsulation, like electro-polymerization, photopolymerization, sol-gel process, and microencapsulation (Nguyen and Kim, 2017).

4) Cross-linking

Cross-linking is an irreversible process of creating three-dimensional enzyme clusters through intermolecular covalent bonds with the addition of a multifunctional reagent (for example, glutaraldehyde). There are two types of cross-linking: cross-linking enzyme aggregate (CLEA)

and cross-linking enzyme crystal (CLEC). Both methods require the use of glutaraldehyde and the presence of amino groups of lysine residues. The main difference is that CLEA is conducted in aqueous media, while for CLEC, enzymes must be priorly crystalized. The advantages of cross-linking are the minimal loss of enzyme molecules and the possibility of microenvironment adjustment *via* stabilizing reagents. However, glutaraldehyde can cause conformational changes and modifications, that would result in loss of activity. Therefore, proteins (BSA/gelatine) are added to the reaction to minimize this effect (Nguyen and Kim, 2017).

Immobilized enzymes have been used in various and broad applications such as waste treatment, clarification, and debittering processes in the food industry, pharmaceutical, chemical, and medical industries, pre-treatment of lignocellulosic materials, and fuel production (Almeida et al., 2022).

Given the importance of enzyme immobilization, it has been the focus of many studies over the years. A bibliometric analysis of the global scientific production of publications on this topic shows how, from 1991 to 2017, the number of publications increased from 50 to 650 per year. Also, according to the database of the Web of Science, more than 2500 publications on enzyme immobilization were published from 2018-2022, which shows the high interest of researchers in this field (Gonçalves et al., 2019).

2.2.1. Immobilization carriers

In most cases, immobilization of biocatalysts is done with various carriers which have specific characteristics such as 1) large specific surface area, 2) good mechanical strength, 3) enhanced stability during the reaction, 4) no interference with the active site of the enzyme, 5) non-toxicity, 6) production sustainability, 7) availability, *etc*. (Xie et al., 2022).

As described by Spasojevic et al. (2020), carriers used in the immobilization of enzymes can be divided into two groups: 1) inorganic carriers and 2) organic carriers.

Inorganic carriers are known to have a stable structure and are inert to the reaction conditions (high pressure, temperature), but they have limited possibilities to create different geometrical shapes. The most commonly used inorganic carriers in enzyme immobilizations are silica and inorganic oxides, mineral materials, and carbon-based materials. Recently, a novel group of inorganic carriers, for example, magnetic nanoparticles, ceramics, graphene oxide, graphene, and carbon nanotubes, have been developed and show great potential. The organic carriers, as

compared to inorganic carriers, exhibit better performance, better immobilization efficiency, and provide higher stability of enzymes during immobilization, but less stability in a harsh environment.

Organic carriers can be divided into two subgroups: 1) biopolymer- and 2) synthetic polymer-based carriers. Biopolymers are defined as natural, biocompatible, non-toxic, and biodegradable materials obtained from sustainable resources. Due to their origin, they show great affinity for enzymes, and most importantly, they preserve the structure and properties of the bound enzyme. It is known that these materials can easily form gels that allow enzymes to be microencapsulated. Commonly used biopolymers are alginates, chitosan, chitin, cellulose, inertness pectin, starch, collagen, and agarose (Figure 3.).

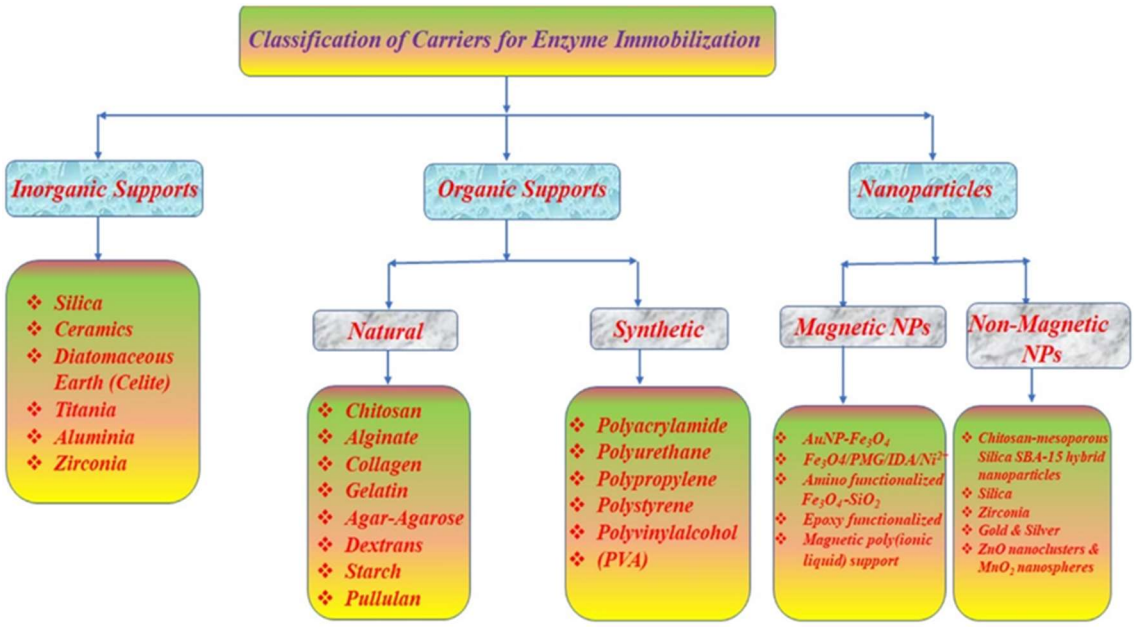

Figure 3. Classification of the carriers for enzyme immobilization: inorganic supports; organic supports, further classified into natural and synthetic supports; and nanoparticles (Aggarwal et al., 2021).

2.2.1.1. Agarose

Agarose is a neutral gelling heteropolysaccharide and contributes to the major fraction of agar. The backbone structure of agarose is a linear polymer with repeating units, that contains both α- and β-glycosidic bonds. The two monosaccharides are β-D-galactose and 3,6-anhydro-α-L-galactose, linked by glycosidic bonds β(1–4) (disaccharide unit called neoagarobiose) and α(1–3) (disaccharide basic unit called agarobiose). Agarose gels can be easily prepared in bead

forms, such as microspheres, whose size and porosity can be easily manipulated during the preparation procedure. With the given data on the usage of agarose beads in enzyme immobilization, it is evident that these beads represent a versatile tool, both on a laboratory scale and in technological applications (Zucca et al., 2016).

2.2.1.2. Polymethacrylates

Polymethacrylates are synthetic linear copolymers prepared with free-radical polymerization. Depending on the starting monomers for preparation, they can be cationic, anionic, or neutral (non-ionic) polymers. The application of such polymers depends on their structure and ionic charge. In a lot of procedures, this kind of polymers can be imprinted with metal ions (in our case, copper ions). One of them was described by Hoai and Kim (2009).

2.3. **Linkers**

Linker molecules generally connect protein elements, maintaining inter-domain interactions and preserving biological activity. In the context of fusion proteins, linkers are reported to improve the stability/folding of proteins, increase expression levels, improve biological activity and alter the pharmacokinetic (PK) profiles of fusion proteins (Chen et al., 2013). This is achieved with the use of inter-domain linkers (specifically α-helical linkers) that function as rigid spacers, preventing unwanted interactions between protein domains during folding (George and Heringa, 2002). To overcome the drawbacks of enzyme immobilization, linear peptides can be used to create a distance between the carrier and the biocatalyst. Theoretically, this approach could lower the probability of unwanted interactions between the carrier and enzyme; therefore, undesired activity loss can be avoided if the insertion of the linker does not interfere with the enzyme conformation.

2.3.1. Natural linkers

Linkers can be defined as linear peptides, which, in naturally occurring multi-domain proteins, bind the functional domains together. In addition, they provide other functions like maintaining cooperative inter-domain interactions or preserving biological activity. In their study, George and Heringa (2002) described some properties of natural linkers, wherein natural linkers have an average length of 10.0 ± 5.8 residues and their hydrophobicity decreases with the increase of linker length. Also, the research suggests that some amino acids, *i.e.* proline, threonine, and glutamine, occur in almost every natural linker. Natural linkers form various conformations in

secondary structures, such as α-helix, β-strand, coil/bend, and turns, depending on their functions. Most linkers on average form α-helix secondary structures (38.3 %), which is a rigid and stable structure, with hydrogen bonds between segments. Linkers with such a structure can also serve as rigid spacers to successfully separate independent protein domains and avoid their interactions if they are not needed. For this reason, this conformation has been adopted by many natural and empirical linkers (Chen et al., 2013).

2.3.2. Empirical linkers

By studying natural multi-domain protein linkers, researchers have designed many empirical linkers with various amino acid sequences and conformations, which are used in many different applications: joining functional domains or releasing them under desired conditions, improving biological activities, achieving controlled or targeted drug delivery, *etc*. (Chen et al., 2013).

2.3.2.1. Flexible linkers

Flexible linkers have a certain degree of movement and/or interaction and good flexibility and solubility. They are mostly applied when the bound domains need a certain degree of movement and interaction (Figure 4.). In most cases, flexible linkers contain specific amino acids such as glycine, serine, and threonine, which allow the linkers to be flexible. A common flexible linker is a "GS-linker" that contains the amino acid sequence of $(Gly\text{-}Gly\text{-}Gly\text{-}Ser)_n/(Gly)$. The length of the linker can be adjusted and optimized depending on its function in fusion proteins (Chen et al., 2013).

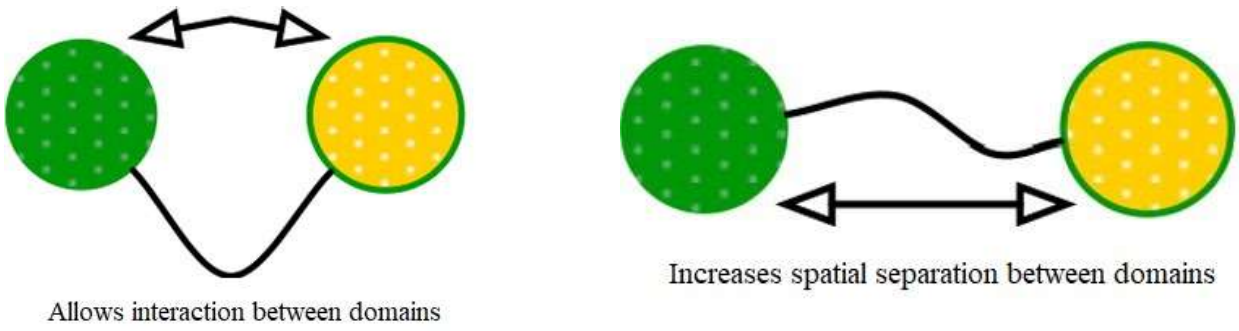

Figure 4. Graphic illustration of flexible linkers and their functions, creating distance and allowing interactions between domains (*according to* Chen et al., 2013)

2.3.2.2. Rigid linkers

Rigid linkers are normally used to maintain a fixed distance between domains of the protein and preserve their independent functions (Figure 5.). These linkers usually exhibit relatively stiff structures and, in most cases, form α-helical structures or contain multiple Pro-residues. An example of the latter linker is a proline-rich non-helix linker with an amino acid sequence $(XP)_n$, where X stands for any amino acid, preferably alanine, lysine, or glutamic acid. A commonly used rigid linker in recombinant fusion proteins is the α-helix linker with the amino acid sequence of $(EAAAK)_n$. The length can be easily adjusted, and in theory, the insertion of such a linker should not have a strong influence on the domains of the protein, so their functions can be preserved. The linker, with various lengths, does not change its properties and structure because the α-helix is under strict structural restraint and its structure is not dependent on the number of repetitions (Chen et al., 2013).

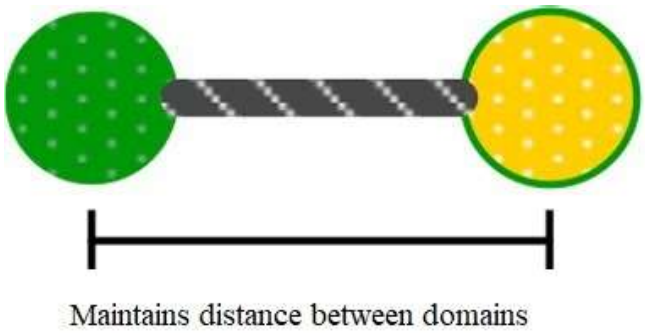

Figure 5. Graphic illustration of the rigid linker and its primary function, preserving distance between protein domains (*according to* Chen et al., 2013)

2.4. Enzyme-linker fusion and immobilization

In most cases, through anchoring enzymes to solid carriers, stability and durability can be gained, but a part of their activity can be permanently lost. In some cases, during the process of immobilization, a certain part of the enzyme would interact with the carriers, where specific bonds are formed. The loss of activity can be explained by the occurrence of unwanted interactions between the support and parts of the enzyme, which are not meant to partake in the immobilization reaction.

As described by Wu et al. (2018), enzyme activity was improved through the insertion of a linker between the enzyme and the support. In this research, a flexible linker was inserted on the C-terminus of the enzyme lysostaphin (Lst), which was then immobilized on different carriers (Figure 6.). The enzyme activity of the naturally occurring Lst and the one with the

inserted linker was measured, and the results indicated that the introduction of a flexible linker greatly enhanced the staphylolytic activity of the immobilized Lst. The immobilized Lst can be re-used and remained active after exposure to 1 % of an organic surfactant C12-14 alcohol ethoxylated (EO) 3:1 sodium sulfate.

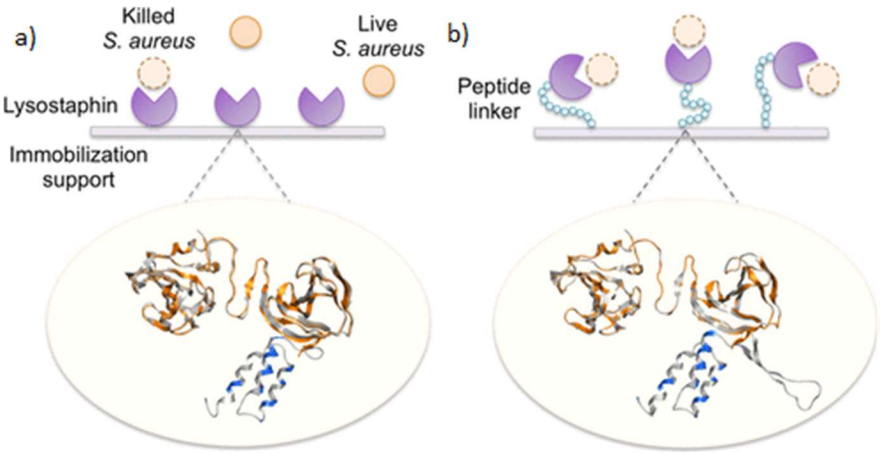

Figure 6. Scheme of Lst immobilization: a) without linker fused, immobilized enzyme molecules were not effective in destroying *S. aureus* cells; b) with flexible linker fused, leading to drastically improved enzyme activity (>99.5% *S. aureus* cells killed) (*according to* Wu et al., 2018)

Yu et al. (2012) described the immobilization of two enzymes [sialyltransferase (*Pm*ST$_1$) from *Pasteurella multocida* and cytidine monophosphate (CMP)-sialic acid synthetase (CSS), from *Neisseria meningitidis*]. The enzymes were fused with a (polyethylene glycol)-N-terminal (PEGylated) cysteine of different lengths and immobilized on magnetic nanoparticles (MNPs) through native chemical ligation. Results showed that with the increase of the PEG linker length between the enzyme and MNPs, the activity also increased when compared to the free enzymes. The authors did not give a detailed explanation, but they indicated the rise in activity might come from non-specific interactions between a fluorescent tag on the substrate and the surface of MNP, while not mentioning any effect from the linkers.

Singh et al. (2018) proposed a different approach to enzyme-linker immobilization and fused magnetite and magnetite core/shell (Fe_3O_4/SiO_2) nanoparticles with two different alkyl chain length linkers (3-phosphonopropionic acid and 16-phosphonohexadeconic acid). The enzyme used was a xylanase (EC 3.2.1.8), which was immobilized on the synthesized bare and silica-coated nanoparticles (Figure 7.). The results showed that the enzymes immobilized through the

longer linker had better catalytic activity and kinetic parameters. Also, enzymes immobilized on silica-coated nanoparticles showed maximum activity when compared to free enzymes and enzymes immobilized on bare nanoparticles. Furthermore, xylanase bound to silica-coated nanoparticles through 16-phosphonohexadeconic acid preserved 90 % of the initial activity after 10 reaction cycles.

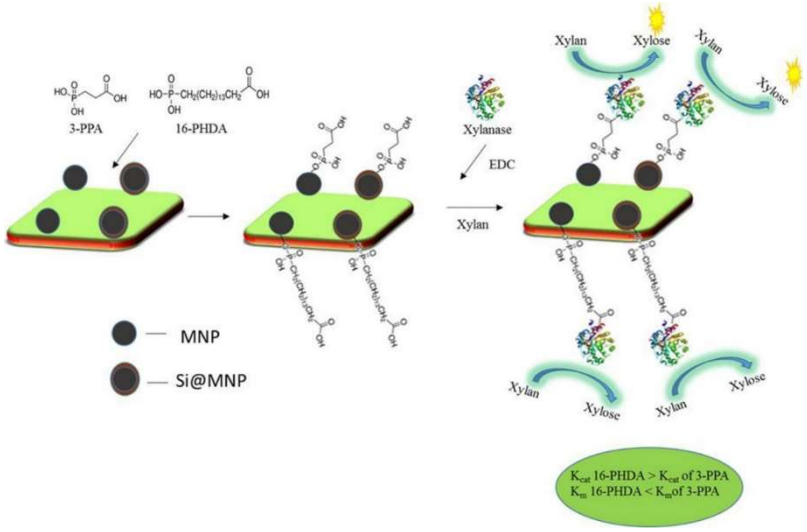

Figure 7. Functionalization of magnetite and magnetite core/shell nanoparticles with 3-phosphonopropionic acid (3-PPA) and 16-phosphonohexadecanoic acid (16-PHDA) acting as linkers for xylanase immobilization through 1-ethyl-3-(3-dimethylaminopropyl)-1-carbodiimide hydrochloride (EDC) coupling. The longer alkyl linker improved the kinetic performance (*i.e.* lower K_m and higher k_{cat}) of the immobilized enzyme as compared to the shorter linker. MNP represents magnetite nanoparticles; Si@MNP represents silica-coated magnetite nanoparticles (Singh et al., 2018)

Moreover, Wang et al. (2022) investigated the fusion of a dehydrogenase with a peptide linker and their immobilization on zeolite imidazolate frameworks-8 (ZIF-8). The results showed a rise in activity of the enzyme-linker molecule after immobilization by 138.7 % and the preservation of 81.2 % of initial activity after seven cycles of the reaction. In addition, the fusion product showed increased catalytic efficiency and stability at 70-80 °C/pH 10-11 compared to free enzymes.

3. EXPERIMENTAL PART

3.1. Materials

In this section, materials and strains for construction and characterization of the fusion complexes of *Lm*SP with His_6-tag on C- (*Lm*SP-His_6) or N- terminus (His_6-*Lm*SP) and different sizes of the rigid linker (L) - $(EAAAK)_n$ where n = 6 (~5 nm), 14 (~10 nm), or 19 (~15 nm), inserted between the *Lm*SP gene and His_6 coding sequence (Table 2.).

Table 2. Constructed *Lm*SP-L and L-*Lm*SP constructs

Constructs		
No.	C-terminally fused	N-terminally fused
1.	*Lm*SP-His_6 (control)	His_6-*Lm*SP- (control)
2.	*Lm*SP-CL_{5nm}	NL_{5nm}-*Lm*SP
3.	*Lm*SP-CL_{10nm}	NL_{10nm}-*Lm*SP
4.	*Lm*SP-CL_{15nm}	

Chapter 3.1.1. shows *E. coli* strains used for plasmid amplification and storage (*E. coli* TOP10), and enzyme expression [*E. coli* BL21(DE3)]. Chapter 3.1.2. shows immobilization carriers. Chapter 3.1.3. lists kits used for DNA extraction and DNA gel purification, Chapter 3.1.4. the column used for affinity chromatography and Chapter 3.1.5. the ultrafiltration devices for desalting and concentration of purified proteins. The medium used for the cultivation of two *E. coli* strains [BL21(DE3) and TOP10] is given in Chapter 3.1.6. Table 3. shows the chemicals and compounds used in this Graduate Thesis, Table 4. shows enzymes used in activity assays (continuous coupled activity assay and discontinuous coupled activity assay), PCR, and POE-PCR. Table 5. displays the buffers used in the purification of *Lm*SP-CL and NL-*Lm*SP constructs, PCR, activity assays (continuous coupled activity assay and discontinuous coupled activity assay), immobilization carrier washing, and enzyme storage. The buffer, dyes, and ladders used in DNA gel electrophoresis are listed in Table 6. Table 7. indicates buffers, protein ladders, dyes, and staining solution used in SDS-PAGE. In Table 8. laboratory devices used are listed. Primers used for the assembly of *Lm*SP-CL and NL-*Lm*SP constructs are given in Table 9. and Table 10, respectively. All buffers were prepared at BIOTE, TU Graz, and pH was adjusted with HCl and NaOH with varying molarity. Buffers were filtered using MF-Millipore® Membrane Filter, 0.45 µm pore size (Sigma-Aldrich; St. Louis, USA).

3.1.1. Cultures

Two different strains of *Escherichia coli* were used - *E. coli* TOP10 for plasmid amplification and storage, and *E. coli* BL21(DE3) for enzyme expression. Both strains are stored in the Institute of Biotechnology and Biochemical Engineering (BIOTE), Graz University of Technology (TU Graz).

3.1.2. Immobilization materials

- Cu^{2+} functionalized polymethacrylate-based, epoxy-activated support (size 150 μm) – SEPABEADS^{TM} EC-EP (Mitsubishi Chemical Corporation; Tokyo, Japan).
- Ni^{2+} functionalized, nitrilotriacetic acid (NTA) modified Superflow carrier (size 60–160 μm) – Ni-NTA Superflow (Qiagen; Hilden, Germany)

3.1.3. Kits used for DNA extraction and DNA gel purification:

- Wizard® Plus SV Minipreps DNA Purification System (Promega Corporation; Madison, USA)
- Monarch® DNA gel purification kit (New England BioLabs; Ipswich, USA)

3.1.4. The column used for protein purification by affinity chromatography:

- HisTrapTM FF crude columns (GE Healthcare; Chicago, USA)

3.1.5. Concentrator tube used for buffer change after protein purification:

- Vivaspin Turbo 30 kDa cut-off concentrator tubes (Sartorius AG; Göttingen, Germany)

3.1.6. The medium used for the cultivation of *E. coli* strains [BL21(DE3) and TOP10]:

- Lysogeny Broth (LB) medium (10.0 g/L peptone; 5.0 g/L yeast extract; 5.0 g/L NaCl)

Table 3. List of chemicals and compounds used in this Graduate thesis

Chemical	**Company**
2-(N-morpholino) ethanesulfonic acid (MES, ≥ 99 %)	Carl Roth GmbH; Karlsruhe, Germany
Agarose	Carl Roth GmbH; Karlsruhe, Germany

Table 3. List of chemicals and compounds used in this Graduate thesis - *continuation*

Chemical	**Company**
Ampicillin (>97 %)	Carl Roth GmbH; Karlsruhe, Germany
Bradford reagent (ROTI® Quant, 5× conc.)	Carl Roth GmbH; Karlsruhe, Germany
D (+)-sucrose (≥ 99.5 %)	Carl Roth GmbH; Karlsruhe, Germany
di-Potassium hydrogen phosphate (K_2HPO_4, ≥ 99 %)	Carl Roth GmbH; Karlsruhe, Germany
di-Sodium hydrogen phosphate (Na_2HPO_4, ≥99,0 %)	Carl Roth GmbH; Karlsruhe, Germany
Distilled water (dH_2O)	BIOTE, TU Graz; Graz, Austria
Dithiothreitol (DTT)	Thermo Fisher Scientific Inc.; Waltham, USA
Deoxynucleotide triphosphate (dNTP)	New England BioLabs; Ipswich, USA
Ethanol (EtOH, 96 %)	Carl Roth GmbH; Karlsruhe, Germany
Ethylenediamine tetraacetic acid disodium salt dihydrate (EDTA, ≥ 99 %)	Carl Roth GmbH; Karlsruhe, Germany
Glucose 1 - phosphate (Glc-1-P, ≥ 98 %)	Carl Roth GmbH; Karlsruhe, Germany
Glucose 1,6 - bisphosphate (Glc-1,6-bP, ≥ 99 %)	Carl Roth GmbH; Karlsruhe, Germany
Hydrogen chloride (HCl, > 99 %)	Sigma Aldrich; St. Louis, USA
Imidazole (≥ 99 %)	Carl Roth GmbH; Karlsruhe, Germany
Isopropyl β-D-1-thiogalactopyranoside (IPTG, ≥ 99 %)	Sigma Aldrich; St. Louis, USA
Magnesium chloride ($MgCl_2$, ≥ 99 %)	Carl Roth GmbH; Karlsruhe, Germany
3-(N-morpholino)-propane sulphonic acid	Carl Roth GmbH; Karlsruhe, Germany
Nano-pure water (ddH_2O)	BIOTE, TU Graz; Graz, Austria
Nickel(II) sulfate	Carl Roth GmbH; Karlsruhe, Germany
Nicotinamide adenine dinucleotide (NAD^+, > 98 %)	Carl Roth GmbH; Karlsruhe, Germany
PCR primers	Integrated DNA Technologies Inc.; Coralville, USA
Peptone (Casein)	Carl Roth GmbH; Karlsruhe, Germany

Table 3. List of chemicals and compounds used in this Graduate thesis - *continuation*

Chemical	Company
Potassium dihydrogen phosphate (KH_2PO_4, ≥ 99 %)	Carl Roth GmbH; Karlsruhe, Germany
SDS loading solution	Thermo Fisher Scientific Inc.; Waltham, USA
Sodium chloride (NaCl, ≥ 99.5 %)	Carl Roth GmbH; Karlsruhe, Germany
Sodium hydroxide (NaOH, ≥ 99 %)	Carl Roth GmbH; Karlsruhe, Germany
Yeast extract	Carl Roth GmbH; Karlsruhe, Germany

Table 4. Enzymes used in PCR, POE-PCR, and activity assays (continuous coupled activity assay and discontinuous coupled activity assay)

Enzyme	Company
Glucose 6 - phosphate dehydrogenase (G6P-DH)	Sigma Aldrich/Merck; Darmstadt, Germany
Phosphoglucomutase (PGM)	Sigma Aldrich/Merck; Darmstadt, Germany
PrimeSTAR polymerase (POE-PCR)	TAKARA; Kusatsu, Japan
Q_5 polymerase (PCR)	New England BioLabs; Ipswich, USA

Table 5. Buffers used for purification of *Lm*SP-His_6, *Lm*SP-CL, and NL-*Lm*SP constructs, PCR, activity assays (continuous coupled activity assay and discontinuous coupled activity assay), and immobilization carrier washing (Chapter 3.1.2.) and enzyme storage

Buffer	Composition/Company
His-trap binding buffer (A)	50.0 mmol/L NaH_2PO_4 300.0 mmol/L NaCl 10.0 mmol/L imidazole pH 7.4
His-trap elution buffer (B)	50.0 mmol/L NaH_2PO_4 300.0 mmol/L NaCl 300.0 mmol/L imidazole pH 7.4

Table 5. Buffers used for purification of *Lm*SP-His_6, *Lm*SP-CL, and NL-*Lm*SP constructs, PCR, activity assays (continuous coupled activity assay and discontinuous coupled activity assay), and immobilization carrier washing (Chapter 3.1.2.) and enzyme storage - *continuation*

Buffer	**Composition/Company**
His-trap stripping buffer	20.0 mmol/L Na_2HPO_4 500.0 mmol/L NaCl 50.0 mmol/L EDTA pH 7.0
Q_5® (5×) reaction buffer	New England Biolabs; Ipswich, USA
Buffer for continuous coupled activity assay	50.0 mmol/L potassium phosphate 10.0 mmol/L $MgCl_2$ 10.0 mmol/L EDTA 10.0 µmol/L Glc-1,6-bP pH 7.0
Buffer for discontinuous coupled activity assay	50.0 mmol/L Tris/HCl 10.0 mmol/L $MgCl_2$ 10.0 mmol/L EDTA 10.0 µmol/L Glc-1,6-bP pH 7.7
Washing/storage buffer	50.0 mmol/L potassium phosphate pH 7.0

Table 6. Buffer, ladders, and dyes used in DNA gel electrophoresis

Buffer/ladder/dye/gel	**Company**
Tris-Acetate-EDTA (TAE) buffer	BIOTE, TU Graz; Graz, Austria
1kb DNA ladder	New England BioLabs; Ipswich, USA
Gel loading dye, Purple, no SDS (6×)	New England BioLabs; Ipswich, USA
HDGreen™ Plus DNA Stain	INTAS; Göttingen, Germany

Table 7. Buffers, protein ladders, gel, and staining solution used in SDS-PAGE

Buffer/protein ladder	**Company**
NuPAGE™ LDS Sample buffer (4×)	Thermo Fisher Scientific Inc.; Waltham, USA
NuPAGE™ MOPS Running buffer	Thermo Fisher Scientific Inc.; Waltham, USA
PageRuler™ pre-stained protein ladder	Thermo Fisher Scientific Inc.; Waltham, USA
Staining solution (0.5 % Coomassie blue, 50.0 % methanol, 10.0 % acetic acid)	BIOTE, TU Graz; Graz, Austria
Destaining solution (30.0 % methanol, 10.0 % acetic acid)	BIOTE, TU Graz; Graz, Austria
NuPAGE™ Bis-Tris Mini Protein Gels	Thermo Fisher Scientific Inc.; Waltham, USA

Table 8. Laboratory devices

Device	**Company**
ÄKTA Prime plus purification system	GE Healthcare; Chicago, USA
Analytical balance LE244S	Sartorius AG; Göttingen, Germany
Centrifuge HiCen SR	Herolab; Wiesloch, Germany
Protein electrophoresis cell Mini-PROTEAN Tetra Vertical Electrophoresis Cell	Bio-Rad; Hercules, USA
DNA electrophoresis cell Mini-Sub Cell GT Cell	Bio-Rad; Hercules, USA
Electroporation device MicroPulser Electroporator	Bio-Rad; Hercules, USA
Falcon-tube centrifuge Centrifuge 5810 R	Eppendorf; Hamburg, Germany
Incubation-shaker cabinet CERTOMAT BS-1	Sartorius AG; Göttingen, Germany
Laboratory balance V1C-612	Acculab; New York, USA
Laminar BioAir AURA-2000 M.A.C.	EuroClone S.p.A.; Milan, Italy

Table 8. Laboratory devices - *continuation*

Device	Company
Lyophilizator/Freeze dryer Christ alpha 1-4	B. Braun Biotech International; Melsungen, Germany
Mini centrifuge Centrifuge 5424 R	Eppendorf; Hamburg, Germany
NanoDrop DS-11	DeNovix Inc.; Wilmington, USA
Plate-reader FLUOstar Omega	BMG Labtech; Ortenberg, Germany
Rotary shaker Rotator SB3	Stuart; Stone, United Kingdom
Sonic Dismembrator Model 505	Thermo Fisher Scientific Inc.; Waltham, USA
Spectrophotometer DU 800	Beckman Coulter; Brea, USA
Thermal cycler Doppio	VWR; Radnor, USA
Thermoblocks SC-24N	Biosan; Riga, Latvia
Vortex V-1-Plus	Biosan; Riga, Latvia
Water bath IKA Heating Bath	Profilab24 GmbH; Berlin, Germany
Water purificator Arium Mini	Sartorius AG; Göttingen, Germany

3.1.7. Primer design

Firstly, a pair of primers [insert gene forward primer (IF) and insert gene reverse primer (IR)] was designed to amplify the DNA fragment-the gene coding for *Lm*SP (GenBank ID: E03420.1). Another pair of primers [vector backbone forward primer (VF) and vector backbone reverse primer (VR)] was designed and used to amplify the vector backbone (plasmid pET21b containing various linkers, synthesized from GenScript, Figure 8.). The VF primer contains the last 25 bases of the *Lm*SP sequence and the 25 bases upstream of the *Nde*I site from the vector. The IF primer contains the 25 bases downstream of the *Xho*I site from the vector and the first 25 bases of the *Lm*SP sequence. The IF and VF sequences are reverse complementary to the VR and IR sequences (Table 9.). For C-terminal linker insertion, three different pairs of primers were designed: primers with sequence $(EAAAK)_6$ (VF6/IR6), primers with sequence $(EAAAK)_{14}$ (VF14/IR14), and primers with sequence $(EAAAK)_{19}$ (VF19/IR19). For N-terminal linker insertion, two different pairs of primers were designed: primers with sequence $(EAAAK)_6$ (VR6/IF6) and primers with sequence $(EAAAK)_{14}$ (VR14/IF14). The detailed

sequence information on the primers used is shown in Table 9. and Table 10.

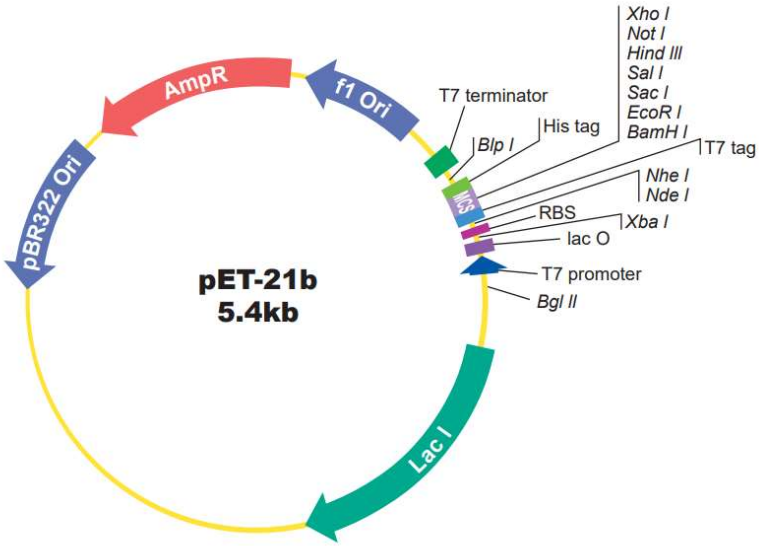

Figure 8. pET-21b vector used in PCR/POE-PCR (Anonymous, 2022)

Table 9. Primers used for construction of *Lm*SP-CL

Primer	Sequence (5'- 3')
IF	ACTTTAAGAAGGAGATATACATATGATGGAAATCCAGAATAAGGCCATG
VR	CATGGCCTTATTCTGGATTTCCATCATATGTATATCTCCTTCTTAAAGT
VF6	AGCAGCGATAATCTGACCCAGAATCTGGCGGAGGCGGCGGCGAAAGAGG
IR6	CCTCTTTCGCCGCCGCCTCCGCCAGATTCTGGGTCAGATTATCGCTGC
VF14	AGCAGCGATAATCTGACCCAGAATCTGGCGGAGGCGGCGGCGAAGGAAGC
IR14	AGCAGCGATAATCTGACCCAGAATCTGGCGGAGGCGGCGGCGAAGGAAGC
VF19	AGCAGCGATAATCTGACCCAGAATCTGGCGGAGGCGGCGGCGAAAGAGG
IR19	CCTCTTTCGCCGCCGCCTCCGCCAGATTCTGGGTCAGATTATCGCTGCT

Table 10. Primers used for construction of NL-*Lm*SP

Primer	Sequence (5'- 3')
VF	AGCAGCGATAATCTGACCCAGAATTAACTCGAGCACCACCACCACCACC
IR	GGTGGTGGTGGTGGTGCTCGAGTTAATTCTGGGTCAGATTATCGCTGCT
IF6	GAAGCGGCGGCGAAGGCGGCGGCGATGGAAATCCAGAATAAGGCCATG
VR6	CATGGCCTTATTCTGGATTTCCATCGCCGCCGCCTTCGCCGCCGCTTC
IF14	GAGGCGGCGGCGAAGGCGGCGGCGATGGAAATCCAGAATAAGGCCATG
VR14	CATGGCCTTATTCTGGATTTCCATCGCCGCCGCCTTCGCCGCCGCCTC

3.2. Methods

3.2.1. Construction of *Lm*SP-CL and NL-*Lm*SP constructs

3.2.1.1. PCR

The *E. coli* TOP10 strains containing the plasmid pET21b-*Lm*SP and pET21b-linkers [without the gene for *Lm*SP, with different linker lengths (5 nm, 10 nm, and 15 nm)] were cultivated at 37 °C overnight in the LB medium. The plasmids were extracted from the cells using a standard DNA extraction kit, Wizard® Plus SV Minipreps DNA Purification System (Promega Corporation; Madison, USA) following the standard protocol. The concentration of the extracted plasmids was around 200 ng/µL, measured with Nanodrop DS-11 (DeNovix Inc.; Wilmington, USA). With the isolated plasmid (template for PCR), the PCR mixture was prepared following the protocol: 5 µL Q_5 buffer, 0.5 µL dNTP solution, 1 µL template (plasmid) solution, 0.25 µL Q_5 polymerase, 1.25 µL primer solutions, and sterilized water to the volume of 25 µL. The PCR conditions used are shown in Table 11.

Table 11. PCR conditions used in *Lm*SP gene and vector backbone (pET21b) amplification

Step	Time	Temperature [°C]	Cycles
Initial Denaturation	30 s	98	1
Denaturation	10 s	98	35
Annealing	30 s	58	
Elongation	1 min	72	
Final Elongation	5 min	72	1

The PCR products were checked by agarose gel electrophoresis (Chapter 3.2.1.3.) using a 1 kb DNA ladder (New England BioLabs; Ipswich, USA) as a reference (Chapter 4.1., Figure 10.). Afterward, the desired fragments were purified using the DNA gel purification kit Monarch® (New England BioLabs; Ipswich, USA) following the standard protocol. The concentration of the vector (pET21b-linkers) and insert fragments (*Lm*SP gene with linker sequences homologous to pET21b-linkers) was checked by using the Nanodrop DS-11 (DeNovix Inc.; Wilmington, USA).

3.2.1.2. POE-PCR

POE-PCR is a simple cloning method in which DNA inserts are subcloned into any location of a vector without the need for a restriction enzyme, exonuclease, ligase, or recombinase (Figure 9.; Zhong et al., 2017). The product of POE-PCR is a DNA multimer, which contains several repetitions of the vector sequence with the inserted gene of interest. POE-PCR was performed using the aforementioned purified vector (pET21b-linkers) and insert fragments (*Lm*SP gene with linker sequences homologous to pET21b-linkers). The PCR mixture, in 25 µL, contained the vector and insert fragments under a molar ratio of 1:1 (12.5 µL in total) and additional 12.5 µL PrimeSTAR polymerase (TAKARA; Kusatsu, Japan). The vector and insert fragment are acting as primers for each other, so no additional primers were added to the mixture. The PCR conditions used are shown in Table 12. The PCR product was further checked by gel electrophoresis (Chapter 3.2.1.3.; Chapter 4.1., Figure 11.).

Table 12. POE-PCR conditions used for DNA-multimer production

Step	Time	Temperature [°C]	Cycles
Initial Denaturation	10 s	98	1
Denaturation	10 s	98	15
Annealing	15 s	57	
Elongation	2.5 min	72	
Denaturation	10 s	98	20
Annealing	15 s	57	
Elongation	4 min	72	
Final Elongation	5 min	72	1

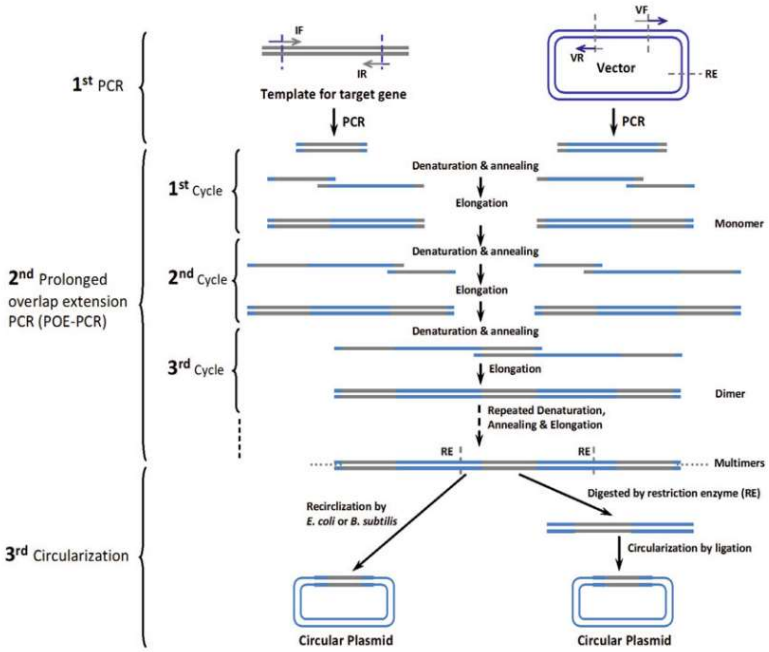

Figure 9. Flow scheme of POE-PCR: 1st – standard PCR reaction, amplification of target gene and vector backbone; 2nd – POE-PCR, creation of DNA-multimers; 3rd – transformation and obtainment of circular plasmids (Zhong et al., 2017)

The multimer was transformed into *E. coli* BL21(DE3) competent cells using electroporation (Chapter 3.2.1.4.) device MicroPulser Electroporator (Bio-Rad; Hercules, USA) and transformed cells were spread on a sterilized LB agar with ampicillin (in final concentration of 100 µg/mL) overnight at 37 °C. The single colonies were picked and incubated in 10 mL of sterilized LB medium containing ampicillin (at a final concentration of 100 µg/mL) overnight. The extraction of the plasmid was done using a DNA extraction kit (Promega Corporation; Madison, USA) following the standard protocol. The concentration of the extracted plasmids was checked with Nanodrop DS-11 (DeNovix Inc.; Wilmington, USA). Sequencing of the plasmids was done afterward.

3.2.1.3. DNA gel electrophoresis

0.5 grams of agarose was dissolved in 50 mL of Tris/acetate (TAE) buffer in an Erlenmeyer flask (microwave heating, 30 s). After agarose was dissolved, DNA staining dye [HDGreen™ Plus DNA Stain (INTAS; Göttingen, Germany), 5 µL] was also added to the suspension. The suspension was poured into the electrophoresis unit with a comb on top, which forms the sample wells. After cooling down the gel for 30 minutes, the comb was removed. The electrophoresis

unit was filled with the appropriate buffer (TAE) until the gel was fully submerged. The DNA samples [1 µL of the sample, 1 µL of the loading dye, Gel loading dye, Purple, no SDS (6×) (New England BioLabs; Ipswich, USA)] and the 1kb DNA ladder (New England BioLabs; Ipswich, USA) were loaded into the gel. The power supply was connected and a constant voltage of 100 V at room temperature was applied for 30 minutes. The power was turned off, the gel was taken out of the unit and placed on a fluorescent lamp. Amplified DNA fragments (bands) were visualized under fluorescence (Chapter 4.1., Figure 10. and Figure 11.).

3.2.1.4. Transformation of bacterial cells

E. coli BL21(DE3) cells were used for transformation that was done using the electroporation (single pulse, 12 kV/cm, 200 Ω, and 25 µF) method using MicroPulser Electroporator (Bio-Rad; Hercules, USA). It increases the permeability of the cell membrane, allowing the plasmid/multimer to be transferred into cells. Transformed cells were incubated at 37 °C for 30 min and transferred to a sterilized LB agar medium and ampicillin (in final concentration of 100 µg/mL). The culture was incubated overnight at 37 °C and stored (+4 °C) for further experiments. Also, in parallel, the transformation of *E. coli* TOP10 cells was done for long-term plasmid storage.

3.2.2. *Lm*SP-His_6, *Lm*SP-CL, and NL-*Lm*SP expression

The *E. coli* BL21(DE3) cells containing plasmids with different linker length sequences fused with the *Lm*SP gene (Table 2.) were grown in LB medium (final concentration of ampicillin 100 µg/mL) at 37 °C, respectively. When the OD, determined at a wavelength of 600 nm (OD_{600}), of the suspension reached a value of 0.6 – 0.8 AU, isopropyl *β*-D-1-thiogalactopyranoside (IPTG) was added into the culture to its final concentration of 0.25 mM to induce protein expression. The expression was done overnight at 18 °C and a shaking speed of 120 rpm.

3.2.3. *Lm*SP-His_6, *Lm*SP-CL, and NL-*Lm*SP purification

After cultivation, cells were harvested [5000 rpm, 4 °C, 20 min; Centrifuge 5810 R (Eppendorf; Hamburg, Germany)], suspended in buffer A (Table 5.), and disrupted by ultrasonication with a Sonic Dismembrator Model 505 (Fisher Scientific Inc.; Waltham, USA) using the following

protocol: 6 min in total, alternating 2 pulses on/4 s pulse off at 60 % amplitude. The cell extract was recovered [15000 rpm, 4 °C, 20 min, HiCen SR (Herolab; Wiesloch, Germany)] and the constructs were purified using pre-packed (1.6 × 2.5 cm; 5 mL) HisTrap™ FF crude columns (GE Healthcare; Chicago, USA) on an ÄKTA Prime plus purification system (GE Healthcare; Chicago, USA). The column was priorly washed with dH_2O and buffer A (Table 5.). The flow rate was set to 2 mL/min of buffer A (Table 5.) and the flow through with unbound proteins was discarded. His-tagged proteins were eluted with an imidazole gradient (0.01-0.3 M) with buffer B (Table 5.). The fractions with significant absorbances at 280 nm were collected in Falcon tubes. The HisTrap™ FF crude column was regenerated with $NiSO_4$, washed with water, and finally with EtOH (20 %). The purified proteins were desalted and concentrated (≥ 15 mg/mL) using Vivaspin Turbo 30 kDa cut-off concentrator tubes (Sartorius AG; Göttingen, Germany) and 50 mM potassium phosphate buffer, pH 7.0 (Table 5.). The purified proteins were checked with SDS-PAGE (Chapter 3.2.4.), and the *Lm*SP-His_6, *Lm*SP-CL, and NL-*Lm*SP concentrations were determined with the Bradford method (Chapter 3.2.6.).

3.2.4. SDS-PAGE

The purified enzyme constructs solution (*Lm*SP-CL and NL-*Lm*SP) solution (1-2 mg/mL, 14 µL) was mixed with 5 µL of SDS-PAGE loading buffer [NuPAGE™ LDS sample buffer (4×) (Thermo Fisher Scientific Inc.; Waltham, USA)] and 1 µL of DTT. The mixtures were heated at 99 °C in a thermoblock for 10 minutes. The samples were cooled down to room temperature, centrifuged [10000 rpm; Centrifuge 5424 R (Eppendorf; Hamburg, Germany)] for 1 minute, and loaded (10 µL) into NuPAGE™ Bis-Tris Mini Protein Gel (Thermo Fisher Scientific Inc.; Waltham, USA). A pre-stained protein ladder PageRuler™ (Thermo Fisher Scientific Inc.; Waltham, USA) was loaded as a reference. The power supply was connected to the electrophoresis unit Mini-PROTEAN Tetra Vertical Electrophoresis Cell (Bio-Rad; Hercules, USA) (anode (+) linked to the bottom reservoir and the cathode (-) linked to the upper reservoir), and a constant voltage of 160 V at room temperature [in NuPAGE™ MOPS Running buffer (Thermo Fisher Scientific Inc.; Waltham, USA)] was applied for around 1.5 hours until the dye front reached the bottom of the gel. The gel was taken out of the unit and placed into a plastic container with the staining solution (Table 7.) for 3-4 hours with gentle agitation. Afterward, the gel was placed into the de-staining solution (Table 7.) with gentle agitation until the protein bands were visible (Simpson, 2006).

3.2.5. Activity of *Lm*SP-His_6, *Lm*SP-CL, and NL-*Lm*SP constructs

The activity was measured using the continuous coupled assay (Chapter 3.2.5.1.) and the discontinuous coupled activity assay (Chapter 3.2.5.2.) (Weinhäusel et al., 1994). SP catalyzes the phosphorolysis of sucrose into α-D-fructose and Glc-1-P. With the addition of phosphoglucomutase (PGM), Glc-1-P is converted into glucose 6-phosphate (Glc-6-P). With glucose-6-phosphate dehydrogenase (G6P-DH), Glc-6-P is oxidized and NADH is generated. NADH absorbs UV light and has a significant absorbance peak at 340 nm, therefore the concentration of this molecule can be measured using a spectrophotometer or plate-reader.

3.2.5.1. Continuous coupled activity assay

The buffer (continuous coupled assay buffer, Table 5.), substrate (1.1 M D (+)-sucrose), co-factor (NAD^+, 20 mg/L), coupled assay enzymes (G6P-DH, PGM), and target enzyme (*Lm*SP-His_6, *Lm*SP-CL, or NL-*Lm*SP) under a series of dilutions were prepared. All reagents and buffer (continuous coupled assay buffer) were freshly prepared. The reaction mixture (380 µL continuous coupled assay buffer, 40 µL NAD^+, 2 µL G6P-DH, 2 µL PGM, 130 µL sucrose) was mixed, preheated at 30 °C in thermoblock for 5 minutes, and pipetted into a glass cuvette. The cuvette was placed into the spectrophotometer DU 800 (Beckman Coulter; Brea, USA) with the temperature control set at 30 °C, with which the device was blanked. Measurement starts with the addition of enzyme solution into the cuvette and lasts for 15 min, where reading was done every 16.8 s. The measurements were done in duplicate. The enzyme activity was calculated from the slope of the initial linear part of the given graph.

3.2.5.2. Discontinuous coupled activity assay

Two buffers: discontinuous coupled assay buffer (Table 5.), and 50 mM potassium phosphate buffer, pH 7.0 (Table 5.), substrate (50 mM D (+)-sucrose), co-factor (NAD^+, 20 mg/L), coupled assay enzymes (G6P-DH, PGM), target enzyme (*Lm*SP-His_6, *Lm*SP-CL or NL-*Lm*SP) under a series of dilutions, and Glc-1-P standards (10-600 µM) were prepared. All the needed reagents and buffers were freshly prepared. The reaction mixture (50 mM D (+)-sucrose, 50 mM potassium phosphate buffer, pH 7.0 (Table 5.), final volume 900 µL) was made in an Eppendorf tube (2 mL) and preheated at 30 °C in thermoblock for 5 minutes. The reaction started in Eppendorf tubes while in the thermoblock with the addition of enzyme solution into the tube (100 µL). Samples (200 µL) were taken every 2, 3, 5, 7, and 9 min. The taken samples were

pipetted into pre-heated (100 °C) empty Eppendorf tubes (1.5 mL) which were afterward placed into water bath IKA Heating Bath (Profilab24 GmbH; Berlin, Germany) (∼100 °C) for 5 minutes. The measurement of the produced NADH was carried out on a plate-reader FLUOstar Omega (BMG Labtech; Ortenberg, Germany). Each well of the 96-well plate was filled with 114 µL of the reaction mixture [12 µL G6P-DH, 12 µL PGM, 60 µL NAD^+ solution, 600 µL discontinuous assay buffer (Table 5)] and with 80 µL of the sample (samples taken every 2, 3, 5, 7, and 9 minutes) using automatic pipettes. The measurement was done in the plate reader at 340 nm for 20 minutes. Additionally, a standard Glc-1-P curve with known concentrations was made. The measurements were done in duplicate. The measurement end-values [for each sample (2, 3, 5, 7, and 9 minutes of the enzyme reaction)] were taken and plotted against time for activity estimation, which was calculated from the slope.

3.2.6. Concentration of *Lm*SP-His_6, *Lm*SP-CL, and NL-*Lm*SP

The concentration of *Lm*SP-His_6, *Lm*SP-CL, and NL-*Lm*SP constructs was measured using the Bradford method (Olson and Markwell, 2007) following the standard protocol. The Bradford reagent (ROTI® Quant, 5×) was diluted (1:5), appropriate *Lm*SP-His_6, *Lm*SP-CL, and NL-*Lm*SP dilutions were obtained, and the reaction mixture was prepared in Eppendorf tubes (1.5 mL). Tubes were filled with 500 µL of the Bradford reagent and 10 µL of *Lm*SP-His_6, *Lm*SP-CL, and NL-*Lm*SP solutions. The tubes were gently shaken and left at room temperature for 5 minutes. A blank sample was prepared the same way, with the addition of 10 µL of water instead of the *Lm*SP-His_6, *Lm*SP-CL, and NL-*Lm*SP solutions. Firstly, the spectrophotometer was blanked and a standard curve was made with a set of BSA samples (1 mg/mL – 62.5 µg/mL) measuring the absorbance at a wavelength of 595 nm. Afterward, the *Lm*SP-His_6, *Lm*SP-CL, and NL-*Lm*SP solutions were measured and their concentration was thus calculated.

3.2.7. Immobilization of *Lm*SP-His_6 and *Lm*SP-CL

3.2.7.1. SEPABEADS™ EC-EP

The first round of immobilization of *Lm*SP-His_6 and *Lm*SP-CL (*Lm*SP-CL_{5nm} and *Lm*SP-CL_{15nm}) was performed on Cu^{2+} functionalized SEPABEADS™ EC-EP (bead size 150 µm) (Mitsubishi Chemical Corporation; Tokyo, Japan). The SEPABEADS™ EC-EP were washed with a 50 mM potassium phosphate buffer, pH 7.0 (Table 5.) two times before immobilization (1 mL). Appropriate dilutions of the purified *Lm*SP-His_6 and *Lm*SP-CL (*Lm*SP-CL_{5nm}, *Lm*SP-

CL_{15nm}) stock (initial protein concentration: *Lm*SP-His_6 =16.25 mg/mL, *Lm*SP-CL_{5nm} = 25.57 mg/mL, *Lm*SP-CL_{15nm} = 19.3 mg/mL) were prepared and different enzyme loadings [100, 500, 1000, 2000 µg in 1 mL of 50 mM potassium phosphate buffer, pH 7.0 (Table 5)] were added to the carrier (100 mg/mL). The tubes were kept for 1.5 h in an end-to-end rotator, Rotator SB3 (Stuart; Stone, United Kingdom) at room temperature. After the immobilization, centrifugation [15000 rpm, 4 °C, 5 min, Centrifuge 5424 R (Eppendorf; Hamburg, Germany)] was performed, and the supernatants were taken for analysis (*Lm*SP-His_6 or *Lm*SP-CL concentration, Chapter 3.2.6.). SEPABEADS^{TM} with immobilized *Lm*SP-His_6 or *Lm*SP-CL (*Lm*SP-CL_{5nm}, *Lm*SP-CL_{15nm}) constructs were afterward washed with 50 mM potassium phosphate buffer, pH 7.0 (Table 5.) (1 mL) and placed for 5 minutes in an end-to-end rotator Rotator SB3 (Stuart; Stone, United Kingdom), at room temperature. Centrifugation [15000 rpm, 4 °C, 5 min, Centrifuge 5424 R (Eppendorf; Hamburg, Germany)] was again performed, and the washes were taken for analysis (*Lm*SP-His_6 or *Lm*SP-CL concentration, Chapter 3.2.6.). The washing of SEPABEADS^{TM} with immobilized *Lm*SP-His_6 or *Lm*SP-CL (*Lm*SP-CL_{5nm}, *Lm*SP-CL_{15nm}) was done two times in total. The immobilization yield of *Lm*SP-His_6 and *Lm*SP-CL (*Lm*SP-CL_{5nm}, *Lm*SP-CL_{15nm}) was calculated using equations [2] and [3] (Chapter 3.3.3.).

3.2.7.2. Ni-NTA Superflow

The second round of immobilization of *Lm*SP-His_6 and *Lm*SP-CL (*Lm*SP-CL_{5nm}, *Lm*SP-CL_{10nm}, and *Lm*SP-CL_{15nm}) was performed on Ni^{2+} functionalized Ni-NTA Superflow (size 60–160 µm) (Qiagen; Hilden, Germany). The Ni-NTA beads were washed with a 50 mM potassium phosphate buffer, pH 7.0 (Table 5.) two times before immobilization (1 mL). Appropriate dilutions of the purified *Lm*SP-His_6 and *Lm*SP-CL (*Lm*SP-CL_{5nm}, *Lm*SP-CL_{10nm}, *Lm*SP-CL_{15nm}) constructs stock (initial protein concentration: *Lm*SP-His_6 =16.25 mg/mL /*Lm*SP-CL_{5nm} = 25.57 mg/mL, *Lm*SP-CL_{10nm} = 24.40 mg/mL, *Lm*SP-CL_{15nm} = 19.30 mg/mL) were made (≈ 2 mg/mL) and added to the different carrier amounts (1, 2, 6, 10 mg/mL). The tubes were kept in an end-to-end rotator, Rotator SB3 (Stuart; Stone, United Kingdom), at room temperature for 1.5 h. Afterward, centrifugation [15000 rpm, 4 °C, 5 min, Centrifuge 5424 R (Eppendorf; Hamburg, Germany)] was performed, and the supernatants were taken for analysis (*Lm*SP-His_6 or *Lm*SP-CL concentration, Chapter 3.2.6.). Ni-NTA Superflow with immobilized *Lm*SP-His_6 or *Lm*SP-CL (*Lm*SP-CL_{5nm}, *Lm*SP-$CL_{10nm,}$ or *Lm*SP-CL_{15nm}) were afterward washed with 1 mL of 50 mM potassium phosphate buffer, pH 7.0 (Table 5.) and placed for 5 minutes in an end-to-end rotator Rotator SB3 (Stuart; Stone, United Kingdom) at room temperature. Centrifugation

[15000 rpm, 4 °C, 5 min, Centrifuge 5424 R (Eppendorf; Hamburg, Germany)] was again performed, and the washes were taken for analysis (*Lm*SP-His_6 or *Lm*SP-CL concentration, Chapter 3.2.6.). The washing of Ni-NTA Superflow with immobilized *Lm*SP-His_6 or *Lm*SP-CL (*Lm*SP-CL_{5nm}, *Lm*SP-CL_{10nm}, *Lm*SP-CL_{15nm}) was done two times in total. Immobilization yield of *Lm*SP-His_6 and *Lm*SP-CL (*Lm*SP-CL_{5nm}, *Lm*SP-CL_{10nm}, and *Lm*SP-CL_{15nm}) was calculated using equations [2] and [3] (Chapter 3.3.3). The immobilized activity was determined with the discontinuous coupled activity assay (Chapter 3.2.5.2.) using Ni-NTA Superflow with immobilized *Lm*SP-His_6 or *Lm*SP-CL (*Lm*SP-CL_{5nm}, *Lm*SP-CL_{10nm}, and *Lm*SP-CL_{15nm}). Immobilization effectiveness was calculated using equations [4] and [5] (Chapter 3.3.4.).

3.2.8. Freeze-drying of Ni-NTA Superflow

An appropriate volume (0.5 mL) of the Ni-NTA Superflow was pipetted into priorly weighed Eppendorf tubes. The beads were washed with nano-pure water (ddH2O) to remove the beads storage solution. The Eppendorf tubes were placed into 50 mL Falcon tubes and connected to the Lyophilizator Christ alpha 1-4 (B. Braun Biotech International; Melsungen, Germany). After approximately 24 h, the Eppendorf tubes were weighted, and the mass of the carrier was calculated using equation [6] (Chapter 3.3.5.).

3.3. Data processing

3.3.1. Protein concentration

A standard curve was made with known protein (BSA) concentrations (62.5 µg/mL - 1 mg/mL). Using M. Excel (Microsoft Corporation, 2010), a graph was made and the linear equation (y = ax + b) was obtained. When the absorbance (at a wavelength of 595 nm) of the solutions with unknown concentration of *Lm*SP-His_6, *Lm*SP-CL (*Lm*SP-CL_{5nm}, *Lm*SP-CL_{10nm}, *Lm*SP-CL_{15nm}) and NL-*Lm*SP (NL_{5nm}-*Lm*SP, NL_{10nm}-*Lm*SP) were obtained, the BSA standard curve was used to estimate the protein concentration.

3.3.2. Activity measurements of *Lm*SP-His_6, *Lm*SP-CL, and NL-*Lm*SP

The activity of *Lm*SP-His_6, *Lm*SP-CL (*Lm*SP-CL_{5nm}, *Lm*SP-CL_{10nm}, *Lm*SP-CL_{15nm}), and NL-*Lm*SP (NL_{5nm}-*Lm*SP) was measured in duplicates, with the results shown as an average value with standard deviation. Both the average value and standard deviation were calculated using M. Excel (Microsoft Corporation, 2010) with the integrated functions (AVERAGE and

STDEV).

3.3.3. Immobilization yield of *Lm*SP-His$_6$ and *Lm*SP-CL

The immobilization yield of *Lm*SP-His$_6$ and *Lm*SP-CL (*Lm*SP-CL$_{5nm}$, *Lm*SP-CL$_{10nm}$, and *Lm*SP-CL$_{15nm}$) was calculated using the following equation:

$$Immobilization\ yield\ [\%] = \frac{E_{immobilized}\ [mg]}{E_{loaded}\ [mg]} * 100 \quad [2]$$

where $E_{immobilized}$ is the amount of *Lm*SP-His$_6$ or *Lm*SP-CL that was immobilized on the carrier [mg], E_{loaded} is the initial amount of *Lm*SP-His$_6$ or *Lm*SP-CL used for immobilization (determined as described in Chapter 3.2.6.).

$E_{immobilized}$ was calculated using the equation below:

$$E_{immobilized}[mg] = E_{loaded}\ [mg] - E_{supernatant}\ [mg] \quad [3]$$

where E_{loaded} is the initial amount of *Lm*SP-His$_6$ or *Lm*SP-CL used for immobilization (estimated as described in Chapter 3.2.6.), $E_{supernatant}$ is the amount of *Lm*SP-His$_6$ or *Lm*SP-CL detected in the supernatant and washed elution after immobilization (estimated as described in Chapter 3.2.6.).

3.3.4. Immobilization effectiveness of *Lm*SP-His$_6$ and *Lm*SP-CL

The immobilization effectiveness of *Lm*SP-His$_6$ or *Lm*SP-CL (*Lm*SP-CL$_{5nm}$, *Lm*SP-CL$_{10nm}$, *Lm*SP-CL$_{15nm}$) was calculated using equation [4].

$$Immobilization\ effectiveness\ [\%] = \frac{Immobilized\ activity\ [\frac{U}{mg_{carrier}}]}{Theoretica\ \ activity\ [\frac{U}{mg_{carrier}}]} \quad [4]$$

where immobilized activity presents the estimated activity of *Lm*SP-His$_6$ or *Lm*SP-CL after immobilization (as determined with the discontinuous coupled activity assay, Chapter 3.2.5.2.), theoretical activity presents the theoretical immobilized activity of *Lm*SP-His$_6$ or *Lm*SP-CL obtained through calculations (equation [5]).

Theoretical activity *Lm*SP-His_6 or *Lm*SP-CL was calculated using the equation below:

$$Theoretical\ activity\ [U] = E_{immobilized}[mg] * Specific\ activity\ [\frac{U}{mg_{enzyme}}] \quad [5]$$

where $E_{immobilized}$ is the amount of *Lm*SP-His_6 or *Lm*SP-CL that was immobilized (calculated by using equation [3]), specific activity is the activity of *Lm*SP-His_6 or *Lm*SP-CL (obtained by using discontinuous coupled activity assay, Chapter 3.2.5.2.)

3.3.5. Mass of Ni-NTA Superflow

The mass of Ni-NTA Superflow agarose beads used in *Lm*SP-His_6 or *Lm*SP-CL (*Lm*SP-CL_{5nm}, *Lm*SP-CL_{10nm}, *Lm*SP-CL_{15nm}) immobilization was calculated using this equation:

$$Ni - NTA\ Superflow\ agarose\ beads\ mass\ [mg] = m_2[mg] - m_1\ [mg] \quad [6]$$

where m_2 is the mass of the Eppendorf tube with freeze-dried Ni-NTA Superflow (0.5 mL), m_1 is the mass of the Eppendorf tube.

4. RESULTS AND DISCUSSION

The fusion of α-helix linker [$(EAAAK)_n$; in varying lengths] and *Lm*SP, as well as *Lm*SP immobilization on different carriers, are discussed in this chapter. Construction of fusion complexes was based on POE-PCR (Chapter 3.2.1.2.), and all the PCR products (Chapter 3.2.1.1.) were checked using agarose DNA gel electrophoresis (Chapter 3.2.1.3.). Enzyme expression (Chapter 3.2.2.) and purification (Chapter 3.2.3.) was checked by SDS-PAGE (Chapter 3.2.4.); immobilization efficiency was determined based on the Bradford method (protein concentration assay, Chapter 3.2.6.) and the continuous coupled activity assay (Chapter 3.2.5.1.)/discontinuous coupled activity assay (Chapter 3.2.5.2.). A comparison between the *Lm*SP-His_6, *Lm*SP-CL, and NL-*Lm*SP, regarding activity and immobilization efficiency, was designed to reveal the influence of the inserted linker on enzyme activity and immobilization.

4.1. Construction of *Lm*SP-CL and NL-*Lm*SP

Firstly, primers for standard PCR and POE-PCR were designed as described before (Chapter 3.1.7.). In total, 14 primers were used-eight primers for C-terminal linker insertion (Table 9.) and six primers for N-terminal linker insertion (Table 10.). The plasmids (pET21b-*Lm*SP and pET21b-linkers) were isolated from the *E. coli* TOP10 strain, which was grown at 37 °C overnight, using a standard DNA-extraction kit (Promega Corporation; Madison, USA). Regarding PCR of the primers and the plasmids, firstly, standard PCR (Chapter 3.2.1.1.) was performed to amplify the insert gene and vector backbone. The size of the insert genes without/with linker sequences was approximately 1600 bp (Figure 10.). Secondly, POE-PCR was performed in order to include the linkers to the N- or C- terminus. The amplified vector and inserted genes had overlapping regions on 5' and 3' ends, enabling their usage in POE-PCR (Chapter 3.2.1.2.) without additional primers. Through POE-PCR, DNA multimers containing repeating units of the vector fused with the gene for *Lm*SP with linker sequences were generated, and the resulting constructs had characteristic size, and therefore they could not diffuse through the agarose gel, as shown in Figure 11. The DNA-multimers were transformed into *E. coli* BL21(DE3) *via* electroporation (Chapter 3.2.1.4.). After that, *E. coli* BL21(DE3) hosts cleaved the DNA multimers into desired circular plasmids. The *E. coli* BL21(DE3) cells (grown on LB agar medium) amplified the plasmids that are afterward isolated and sequenced.

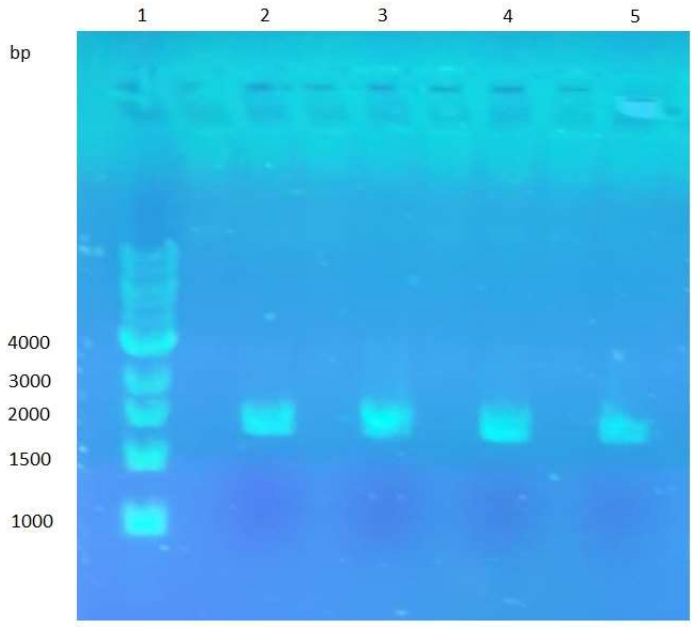

Figure 10. Agarose gel electrophoresis (1 %) of PCR fragments of *Lm*SP genes with a homologous sequence of vector/backbone. Lane 1: 1 kb DNA ladder (New England BioLabs; Ipswich, USA); lane 2: *Lm*SP gene fused with linker sequence $(EAAAK)_6$ on C-terminus; lane 3: *Lm*SP gene fused with linker sequence $(EAAAK)_{14}$ on C-terminus; lane 4: *Lm*SP gene fused with linker sequence $(EAAAK)_6$ on N-terminus; lane 5 - *Lm*SP gene fused with linker sequence $(EAAAK)_{14}$ on N-terminus.

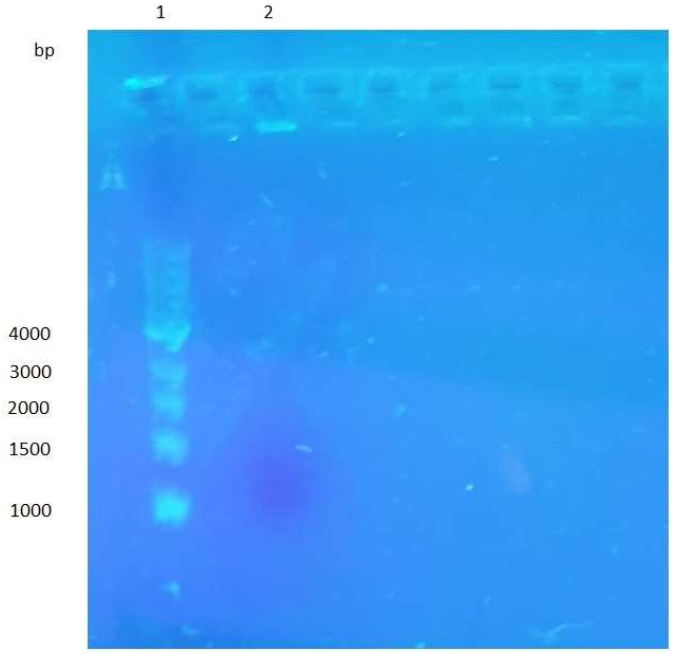

Figure 11. Agarose gel electrophoresis (1 %) of POE-PCR product. Lane 1: 1 kb DNA ladder (New England BioLabs; Ipswich, USA); lane 2: DNA-multimer, unable to diffuse through the agarose gel.

4.2. Expression of *Lm*SP-His_6 and *Lm*SP-CL, and NL-*Lm*SP

E. coli BL21(DE3) strain was used for *Lm*SP-His_6, *Lm*SP-CL, and NL-*Lm*SP expression, due to its high level of expression of the target protein and the lack of proteases that prevents degradation. *E. coli* BL21(DE3) cells were cultivated in LB medium, at 37 °C on a shaker (120 rpm), until the OD_{600} value of 0.6 – 0.8 AU. After that, IPTG (0.25 mM) was added to induce expression of *Lm*SP-His_6, *Lm*SP-CL, and NL-*Lm*SP (Chapter 3.2.2). The *Lm*SP gene was cloned downstream of the T7 promoter within the vector, therefore IPTG induces the expression of the T7 RNA polymerase (under the lacUV5 promoter), which ultimately enables the transcription of the gene of interest. Also, as *E. coli* BL21(DE3) cells are not naturally resistant to ampicillin, only transformed cells can grow in LB media with the addition of ampicillin (0.1 mg/mL).

After protein expression, purification of *Lm*SP-His_6, *Lm*SP-CL, and NL-*Lm*SP was performed, purity and protein size were estimated by SDS-PAGE (Chapter 3.2.4., Figure 13.). The purified *Lm*SP-His_6 had a molecular weight of approximately 55 kDa, matching its calculated molecular mass from the amino acid sequence. Based on concentration of the purified protein, it seems that the insertion of the linker (5 nm) to the N-terminus of *Lm*SP (NL_{5nm}-*Lm*SP) dramatically decreased its soluble concentration level (~10-fold lower) as compared to that of the *Lm*SP and its C-terminally fused complex, which gave ~100 mg enzyme/L culture (Table 18.). According to the crystal structure of *Lm*SP (UniProt Q59495, Figure 12.), its N-terminal area is embedded inside the protein structure, and it is reasonable that the fixing of a rigid linker at the N-terminus would cause the incorrect folding of the enzyme, resulting in the formation of inclusion bodies, and therefore leads to a decreased soluble concentration level (Georgiou and Valax, 1996). On the other hand, the C-terminal fusion (of a 5 nm linker) could maintain the expression level of *Lm*SP (~100 mg enzyme/L culture), and a high-intensity protein band at approximately 58 kDa was obtained after purification of *Lm*SP-CL_{5nm} (Figure 13.b, lane 3), indicating correct folding of the protein. These results, therefore, suggested that the C-terminal linker insertion could be more favourable for *Lm*SP regarding its further improvement and application, and the focus was shifted to the *Lm*SP-CL constructs.

Afterward, using the same protocol as described above (the purification and SDS-PAGE), three constructs of *Lm*SP with different linker lengths (*Lm*SP-CL_{5nm}, *Lm*SP-CL_{10nm} and *Lm*SP-CL_{15nm}) were obtained (Figure 13.). The size of *Lm*SP-CL_{10nm} and *Lm*SP-CL_{15nm} was approximately 62 kDa (Figure 13.b, lane 7) and 65 kDa (Figure 13.b, lane 4), with comparable expression levels as to *Lm*SP-His_6 in the range of 100-150 mg protein/L culture.

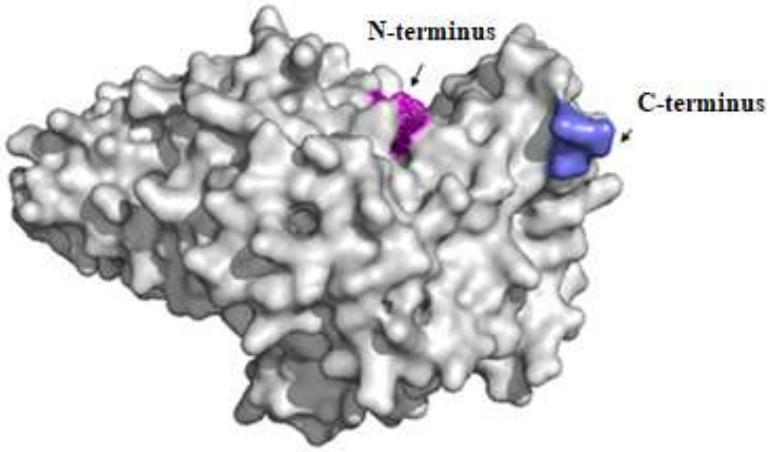

Figure 12. 3D structure of the *Lm*SP (UniProt Q59495, AF-Q59495-F1-model_v3.pdb), showing the position of the N- and C-terminus. The structure was prepared by using PyMOL (Schrödinger LLC, 2022)

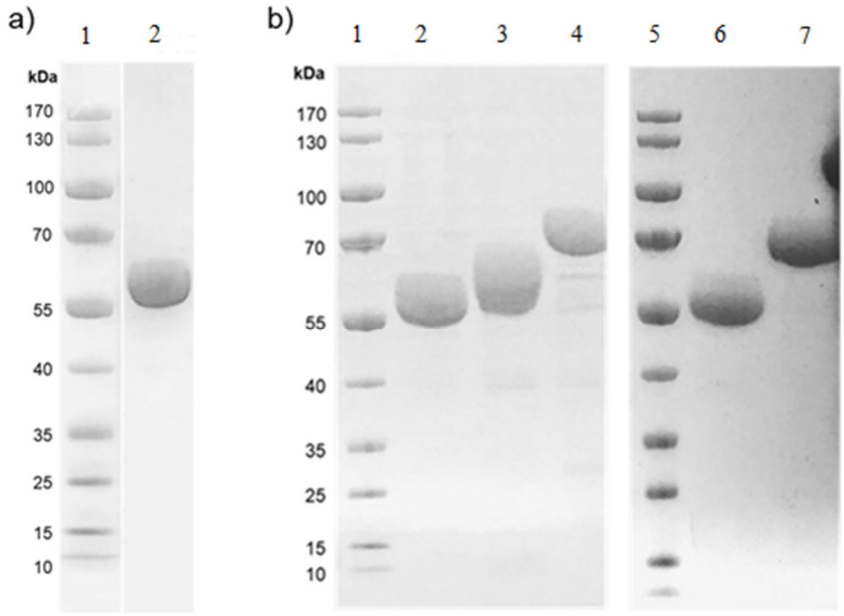

Figure 13. SDS-PAGE of the purified proteins: a) Lane 1: pre-stained protein ladder PageRuler^{TM} (Thermo Fisher Scientific Inc.; Waltham, USA); lane 2: *Lm*SP-His_6; and b) Lanes 1 and 5: pre-stained protein ladder PageRuler^{TM} (Thermo Fisher Scientific Inc.; Waltham, USA); lane 2: *Lm*SP-His_6; lane 3: *Lm*SP-CL_{5nm}; lane 4: *Lm*SP-CL_{15nm}; lane 6: *Lm*SP-His_6; lane 7: *Lm*SP-CL_{10nm}.

4.3. *Lm*SP-His_6, *Lm*SP-CL and NL-*Lm*SP activity

4.3.1. *Lm*SP with linker on N-terminus

The activity of the *Lm*SP construct (NL_{5nm}-*Lm*SP) was determined. Results indicated that the N-terminal insertion of the linker not only affected the folding of molecules (as mentioned above) but also influenced the activity of *Lm*SP. As an example, shown in Table 13., NL_{5nm}-*Lm*SP showed a phosphorolysis activity of 52.3 ± 2.8 U/mg (n=3) as estimated by the continuous coupled activity assay (Chapter 3.2.5.1.). The activity was only 35 % of that from *Lm*SP without a linker inserted [the control; 151 U/mg, measured in the current study but also comparable to published data (Goedl et al., 2007; Koga et al., 1991)]. It's reasonable that the N-terminal rigid peptide linker, especially one facing the inner part of the enzyme, changes the configuration of the protein to some extent, resulting in improper folding and ultimately leading to a decreased activity of the misfolded enzyme. Overall, the N-terminal fusion of the linker turned out to be undesirable for *Lm*SP, and the following investigation focused on the C-terminally fused linkers.

Table 13. Continuous coupled activity assay results for NL_{5nm}-*Lm*SP

Dilution (fold)	Measured activity [U/mL]	Activity [U/mL]	Protein concentration [mg/mL]	Specific activity [U/mg_{enzyme}]	Specific activity [U/mg_{enzyme}]
1000 ×	0.122	122.0	2.2	55.5	52.3 ± 2.8
1500 ×	0.074	111.0		50.5	
2000 ×	0.056	112.0		50.9	

4.3.2. *Lm*SP with linker on C-terminus

Activity analysis was done with the purified *Lm*SP-His_6 and the *Lm*SP constructs with linkers fused to the C-terminal (*Lm*SP-CL). The activity was checked with the continuous coupled activity assay (Chapter 3.2.5.1.) and, in parallel, checked with the discontinuous coupled activity assay (Chapter 3.2.5.2). Detailed data analysis was shown in Tables 14.-17., and overall summarized in Table 18. Results from Table 14. and Table 15. suggest that the *Lm*SP-His_6 had higher specific activity when measured with the discontinuous coupled assay. As compared to the continuous coupled assay using a spectrophotometer that acquires data every 16.8 s, the discontinuous coupled assay could be less accurate. Nevertheless, both methods have shown comparable results, indicating repeatable measurements in the current study. Accordingly, activity measurement of the three *Lm*SP-linker constructs (*Lm*SP-CL_{5nm}, *Lm*SP-CL_{10nm}, and

*Lm*SP-CL_{15nm}) was performed, and the results are summarized in Table 16. and Table 17.

Table 14. Continuous coupled activity assay results for *Lm*SP-His_6

Dilution (fold)	Measured activity [U/mL]	Activity [U/mL]	Protein concentration [mg/mL]	Specific activity [U/mg_{enzyme}]	Specific activity [U/mg_{enzyme}]
5000 ×	0.479	2395.0	16.3	146.9	151.1 ± 5.4
8000 ×	0.304	2432.0		149.2	
10000 ×	0.256	2560.0		157.1	

Table 15. Discontinuous coupled activity assay results for *Lm*SP-His_6

Dilution (fold)	Measured activity [U/min]	Activity [U/mL]	Protein concentration [mg/mL]	Specific activity [U/mg_{enzyme}]	Specific activity [U/mg_{enzyme}]
55000 ×	0.053	2915.0	16.0	182.2	167.0 ± 16.9
170000 ×	0.016	2720.0		170.0	
340000 ×	0.007	2380.0		148.8	

Table 16. Summary of continuous coupled activity assay results for *Lm*SP-His_6 and *Lm*SP-CL constructs

	Measurement 1	Measurement 2	Measurement 3	
	Specific activity [U/mg_{enzyme}]			Specific activity [U/mg_{enzyme}]
*Lm*SP-His_6	146.9	149.2	157.1	151.1 ± 5.4
*Lm*SP-CL_{5nm}	72.3	83.6	81.9	79.3 ± 6.1
*Lm*SP-CL_{10nm}	98.3	111.2	111.8	107.1 ± 7.7
*Lm*SP-CL_{15nm}	96.2	113.5	85.2	98.3 ± 14.3

Table 17. Summary of discontinuous coupled activity assay results for *Lm*SP-His_6 and *Lm*SP-CL constructs

	Measurement 1	Measurement 2	Measurement 3	
	Specific activity [U/mg_{enzyme}]			Specific activity [U/mg_{enzyme}]
*Lm*SP-His_6	182.2	170.0	148.8	167.0 ± 16.9
*Lm*SP-CL_{5nm}	104.4	94.9	/	99.7 ± 6.7
*Lm*SP-CL_{10nm}	110.8	105.7	103.7	106.7 ± 3.6
*Lm*SP-CL_{15nm}	91.8	116.3	/	104.1 ± 17.3

Table 18. Summary of *Lm*SP-His_6 and *Lm*SP-CL constructs expression level and specific activity

Constructs	Structure	Expression level [$mg_{protein}/L_{culture}$]	Specific activity [U/mg_{enzyme}][1]	Specific activity [U/mg_{enzyme}][2]
*Lm*SP-His_6	*Lm*SP-His_6	150-170	167.0 ± 16.9	151.1 ± 5.4
*Lm*SP-CL_{5nm}	*Lm*SP-$(EAAAK)_6$-His_6	~100	99.7 ± 6.7	79.3 ± 6.1
*Lm*SP-CL_{10nm}	*Lm*SP-$(EAAAK)_{14}$-His_6	~150	106.7 ± 3.6	107.1 ± 7.7
*Lm*SP-CL_{15nm}	*Lm*SP-$(EAAAK)_{19}$-His_6	~100	104.1 ± 17.3	98.3 ± 14.3

[1]: activity checked using the discontinuous coupled assay
[2]: activity checked using the continuous coupled activity assay

As seen in Table 18., the expression level and soluble concentration of C-terminally fused *Lm*SP constructs were higher (~100-150 $mg/L_{culture}$) than N-terminally fused *Lm*SP constructs (<10 $mg_{protein}/L_{culture}$). Nevertheless, the *Lm*SP-His_6 showed the highest expression level (~170 $mg_{protein}$/L culture), suggesting that the insertion of a rigid linker either on the C-/N- terminus could affect the expression of *Lm*SP. Overall, the *Lm*SP-CL constructs with slightly decreased expression levels were considered suitable for further applications and investigations due to their activity and solubility (data not shown).

The summary of activity from *Lm*SP-His_6 and *Lm*SP-CL constructs indicated that C-terminal insertion of the linkers also decreased the activity of *Lm*SP. The activities of *Lm*SP-CL_{5nm}, *Lm*SP-CL_{10nm}, and *Lm*SP-CL_{15nm} constructs were lower (by ~35 %) compared to *Lm*SP without linker (*Lm*SP-His_6). This could also be explained by the configuration changes due to the fusion of linkers even though they are not facing the inside of the protein. Interestingly, the *Lm*SP-CL_{5nm}, with the shortest linker inserted, showed the lowest activity among the *Lm*SP-CL constructs, indicating that the length of the linker might not be the dominant factor affecting the activity. Therefore, the three *Lm*SP-CL constructs with desired expression levels and retained specific activity were used in the immobilization study.

4.4. Immobilization of *Lm*SP-His_6 and *Lm*SP-CL constructs

Transition metal ions such as Zn^{2+}, Cu^{2+}, Ni^{2+}, and Co^{2+} have a strong affinity for histidine and cysteine in aqueous solutions (Passerini et al., 2006; Sundberg and Bruce Martin, 1973). This concept is the basis for immobilized-metal affinity chromatography (IMAC), which uses the aforementioned metal ions fixed on supports to coordinatively bind different proteins from solution (Block et al., 2009). One Cu^{2+} ion can bind up to four imidazole rings, and the

association constant for the following bound imidazole ligand decreases (Çam et al., 2014). Ni^{2+} ions (in Ni-NTA systems) coordinate with nitrilotriacetic acid (NTA) with four valencies, leaving two valencies available for interactions with imidazole rings. For His-tagged protein purification, this ratio was proved to be most successful (Block et al., 2009).

In this research, the His-tagged enzyme immobilization onto metal-ion functionalized carriers (SEPABEADS^{TM} EC-EP with Cu^{2+} ions, and Ni-NTA Superflow with Ni^{2+} ions) follows the principle described above.

4.4.1. SEPABEADS^{TM} EC-EP

4.4.1.1. Immobilization yield

The immobilization of *Lm*SP-His_6 and the corresponding *Lm*SP-CL constructs (*Lm*SP-CL_{5nm}, *Lm*SP-CL_{15nm}) were initially tested on SEPABEADS^{TM} EC-EP, which were pre-functionalized with copper ions (Cu^{2+}). The SEPABEADS^{TM} EC-EP were used for enzyme immobilization for their well-known characteristics described by Brady and Jordaan (2009). Immobilization was performed with three sets of enzymes (*i.e.* *Lm*SP-His_6, *Lm*SP-CL_{5nm}, and *Lm*SP-CL_{15nm}) under different loadings, *i.e.*, 50, 500, 1000, and 2000 µg/mL of protein per 100 mg/mL of SEPABEADS^{TM} EC-EP. Immobilization yield for the three *Lm*SP is shown in Figure 14.

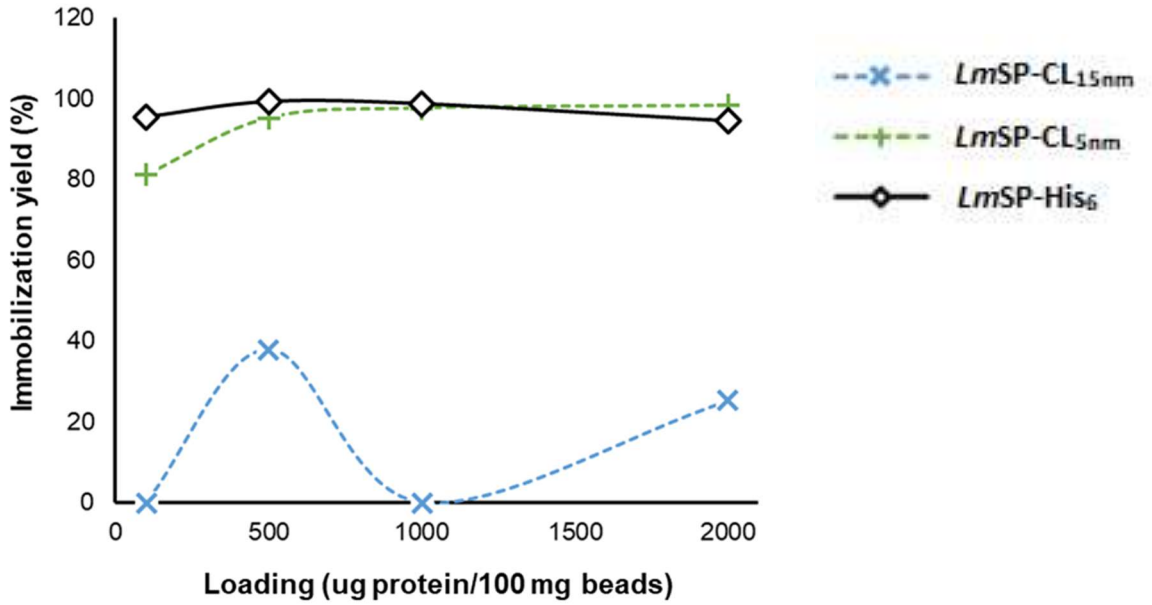

Figure 14. Immobilization yield of *Lm*SP-His_6 and *Lm*SP-CL constructs (*Lm*SP-CL_{5nm} and *Lm*SP-CL_{15nm}) loaded on SEPABEADS^{TM} EC-EP. Immobilization was tested with 50, 500, 1000, and 2000 µg/mL of protein (for each construct) per 100 mg/mL of SEPABEADS^{TM} EC-EP.

As shown in Figure 14., SEPABEADS^{TM} EC-EP showed satisfying immobilization performances, with over 80 % and almost complete immobilization yield being obtained despite the varied protein loading amount, when working with the *Lm*SP-His_6 and *Lm*SP-CL_{5nm}. Notably, no significant decrease in immobilization yield was detected with increasing protein loading concentration, even at the highest level of protein (*i.e.*, 2000 µg/100 mg carrier). Such phenomena were observed in both cases of *Lm*SP-His_6 and *Lm*SP-$CL_{5nm,}$ suggesting that linker insertion did not interfere with the binding between the enzyme and the carrier. It also indicated the high immobilization efficiency when SEPABEADS^{TM} EC-EP was used as a carrier. Indeed, different types of SEPABEADS^{TM} have been widely used for enzyme immobilization with desired results. For example, Nwagu et al. (2012) previously immobilized raw starch digesting amylase (RSDA) onto two SEPABEADS^{TM} (functionalized and non-functionalized) using glutaraldehyde as an activating reagent. The immobilization yield for polyglutaraldehyde (PG) activated carriers was 97 % of the theoretical value. Hilterhaus et al. (2008) immobilized endoglucanase, benzoylformate decarboxylase (BFD) from *Pseudomonas putida*, and lipase B from *Candida antarctica* (*Ca*LB) onto different SEPABEADS^{TM} (EC-EP, EC-EA, and EC-BU). Experiments were carried out with an enzyme loading of ~20 mg/g carrier. Over 85 % yield was obtained for these three enzymes when immobilized on at least one of these SEPABEADS^{TM} EC-EP. Çelem and Önal (2009) immobilized soybean sprout phytase on SEPABEADS^{TM} EC-EP. The experiments were done with four sets of enzyme loadings, where the values were given per gram of the immobilization carrier. With loadings of 1.06 mg, 2.12 mg, 4.24 mg, and 8.48 mg, the immobilization yields were 88.7, 81.6, 77.6, and 72.2 %, respectively. Çelem and Önal, (2022) further tested covalent immobilization of α-galactosidase on SEPABEADS^{TM} EC-EP. The enzyme loading was 1.0 mg/g carrier and an immobilization yield of 90 % was achieved.

However, a dramatic decrease in immobilization yield (below 40 %), as well as an unstable trend against protein loading when the *Lm*SP-CL_{15nm} was loaded on SEPABEADS^{TM} EC-EP, was observed. This could be explained by the larger size of the *Lm*SP construct when fused with a longer linker. According to the structure of *Lm*SP, it has an axial length of approximately 7.5 nm (Figure 15.a). When fused with a linker in the length of ~15 nm, the theoretical maximal length of the construct would be 23 nm. While the SEPABEADS^{TM} EC-EP are described as porous carriers (Figure 16.), with active groups mostly inside and accessible only through pores that have a diameter between of 10 and 20 nm. Therefore, it's plausible that the diffusion of *Lm*SP-CL_{15nm} into beads through pores was spatially inhibited (Figure 15.b), resulting in lower immobilization yield. Occasionally, it can enter the pores if it is oriented properly. In

comparison with *Lm*SP-His_6 and *Lm*SP-CL_{5nm}, diffusion through the pores is not problematic for the constructs with linker ≤ 10 nm (Figure 15.b).

Overall, these results confirmed the rigid structure of the linker fused to the C-terminus of the *Lm*SP, and the porous carriers (SEPABEADS™ EC-EP) turn out to be applicable only for immobilizing the constructs with shorter linkers. To further explore the effect of linker length on enzyme immobilization, the choice of carriers had to be considered.

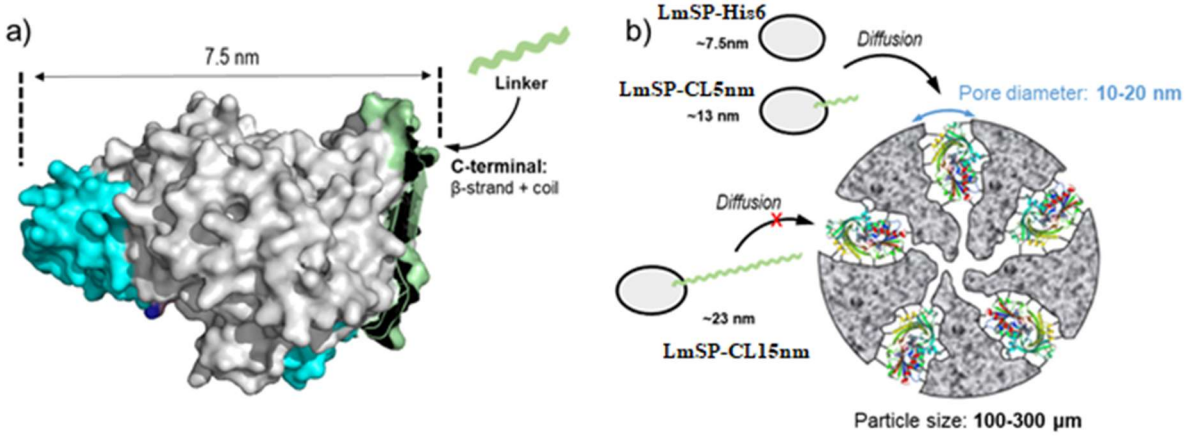

Figure 15. a) Estimated dimension of *Lm*SP based on its protein structure (UniProt Q59495, AF-Q59495-F1-model_v3.pdb). Analysis was done by using PyMOL (Schrödinger LLC, 2022); b) Illustration of *Lm*SP-linker constructs diffusion into SEPABEADS™ EC-EP. SEPABEADS™ EC-EP with pore sizes of 10-20 nm diameter exhibit the diffusion limitation for *Lm*SP-CL_{15nm} (~23 nm).

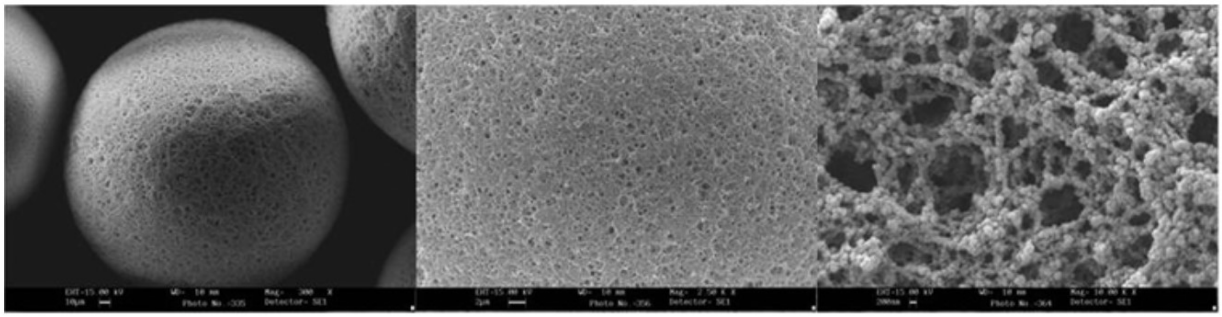

Figure 16. Scanning electron microscope (SEM) graphs of the SEPABEADS™, demonstrating the porousness of this carrier (Hanefeld et al. 2009).

4.4.2. Ni-NTA Superflow

4.4.2.1. Immobilization yield

As an alternative immobilization support, a carrier without pores and having active groups on the surface was designed to eliminate the diffusion issue of the *Lm*SP-CL constructs. The carrier used was Ni-NTA Superflow functionalized with nickel ions (Figure 17.).

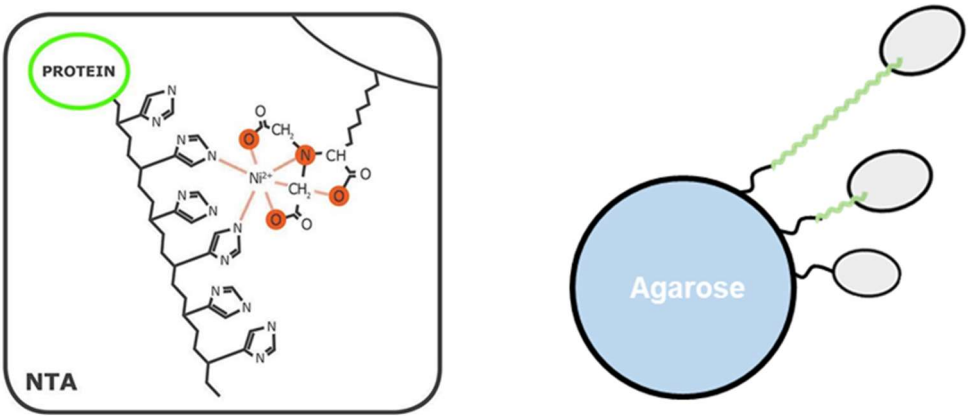

Figure 17. Illustration of enzyme immobilization on Ni-NTA Superflow through interaction between Ni^{2+} ions and histidine (imidazole) residues of proteins (left panel); and the agarose bead with *Lm*SP-linker (in varying lengths) constructs immobilized (right panel).

The Ni-NTA Superflow is generally used as a purification tool for His-tagged proteins due to the high binding capacity (~50 mg protein/mL volume). Kurlemann and Liese (2004) immobilized benzaldehyde lyase onto Ni-NTA carriers, having an immobilization yield of 99 %. In addition, Xu et al. (2022) immobilized recombinant SP from *Bifidobacterium longum* on Ni-NTA agarose spheres, showing enhanced stability and fructose tolerance, with an immobilization yield of 80.2 %.

In the current study, immobilization was performed with four different amounts of Ni-NTA Superflow (1, 2, 6, and 10 mg/mL). *Lm*SP-His_6 and *Lm*SP-CL constructs (*Lm*SP-CL_{5nm}, *Lm*SP-CL_{10nm}, and *Lm*SP-CL_{15nm}) were immobilized at the same loading amount (approximately 2 mg/mL). The results are summarized in Figure 18.

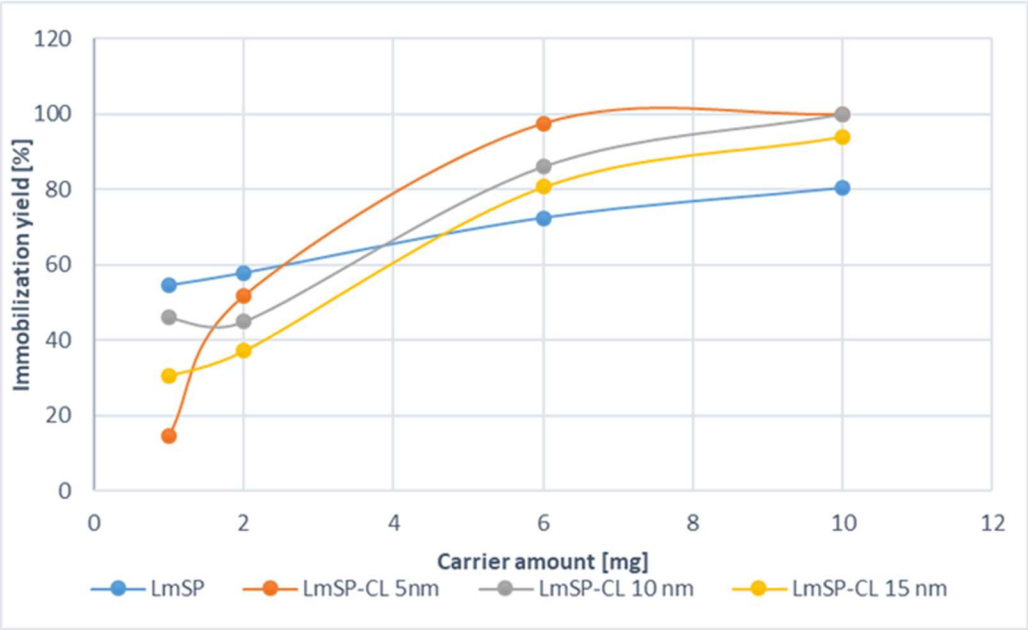

Figure 18. Immobilization yield of *Lm*SP-His_6 and *Lm*SP-CL constructs (*i.e.* *Lm*SP-CL_{5nm}, *Lm*SP-C_{10nm}, and *Lm*SP-C_{15nm}) on Ni-NTA Superflow. Immobilization was performed with approximately the same concentration of *Lm*SP-His_6 and *Lm*SP-CL constructs (~2 mg/mL for each construct) loaded on different concentrations of the Ni-NTA Superflow (1, 2, 6, and 10 mg/mL).

As seen in Figure 18., for all types of enzymes (*Lm*SP-His_6 and *Lm*SP-CL constructs), the immobilization yields increased (up to 100%) with concentrations of the carrier. An immobilization yield of over 40 % was achieved despite the enzyme type, indicating the excellent immobilization performance of the Ni-NTA Superflow. In addition, it was noteworthy that the *Lm*SP-CL constructs had a higher immobilization yield than the control (*Lm*SP-His_6) when higher amounts of the carrier (6 and 10 mg) were used. This could be explained by a higher immobilization density of the *Lm*SP-CL constructs due to the fused linker. With a linker attached, the constructs have a flexible probe to interact with the beads, thus requiring less space to accommodate the protein as compared to the control. Therefore, more molecules can be immobilized, resulting in a higher immobilization yield. Similar results were also reported in the previous studies. For example, Tominaga et al. (2005) used alkaline phosphatase (AP) obtained from *E. coli* for immobilization onto agarose gel beads. Two peptide tags with reactive lysine and with different lengths of Gly-Ser attached to the C- and N-terminus were used. The wild-type AP only had an immobilization yield of 9 %. The insertion of the K6 tag (MKHKGS) on the C-terminus improved immobilization yield slightly (12 %), whereas the insertion of the K6 tag on the N-terminal resulted in an immobilization yield of 36 %. The insertion of the K14

tag [MKHK(GGGS)$_2$GS] on the N-terminus showed the best result, with an immobilization yield of 71 %, suggesting the potential of linkers in enzyme immobilization. Besides, Lu et al. (2022) fused a thermostable β-galactosidase (Tpebgl3) with the linker 4LP [VKTQATSREEPPRLPSKHRPG)$_4$VKTQTAS]. The Tpebgl3 and 4LP-Tpebgl3 were tested on Na-Y zeolite carrier, where the Tpebgl3 achieved a maximum immobilized enzyme concentration of 25.5 ± 1.1 mg/g $_{carrier}$, with an adsorption yield of 32.8 ± 0.8 %. On the other hand, 4LP-Tpebgl3 obtained a maximum immobilized enzyme concentration of 50.3 ± 0.4 mg/g $_{carrier}$, with an adsorption yield of 62.1 ± 0.1 %. Wang et al. (2022) immobilized amino acid dehydrogenase fused with a peptide linker onto the metal-organic framework ZIF-8. The coordination of metal ions with the linker enabled precise orientation of the enzyme immobilization, resulting in higher enzyme loading capacity. Overall, it is plausible that the insertion of a linker benefits the immobilization of enzymes, which shows high potential for future industrial applications.

4.4.2.2. Immobilized activity

In addition to immobilization yield, the activity of the immobilized enzymes is also crucial and needs consideration. Here, the activity of *Lm*SP-His$_6$ and *Lm*SP-CL (*Lm*SP-CL$_{5nm}$, *Lm*SP-CL$_{10nm}$, *Lm*SP-CL$_{15nm}$) (~ 2 mg) loaded on 10 mg of Ni-NTA Superflow, showing the highest immobilization yield (~100 %) for each construct, were measured and shown in Table 19. Accordingly, immobilization effectiveness was calculated and listed in Table 20.

Table 19. Discontinuous assay results for the immobilized *Lm*SP-His$_6$ and *Lm*SP-CL constructs (approximately 2 mg/mL protein for 10 mg/mL Ni-NTA Superflow)

	Measurement 1	**Measurement 2**	**Measurement 3**	
	Immobilized activity [U/mg$_{carrier}$]			**Immobilized activity [U/mg$_{carrier}$]**
*Lm*SP-His$_6$	9.3	10.7	/	10.0 ± 1.0
*Lm*SP-CL$_{5\ nm}$	24.1	21.8	23.7	23.2 ± 1.2
*Lm*SP-CL$_{10\ nm}$	15.0	20.0	16.9	17.3 ± 2.5
*Lm*SP-CL$_{15\ nm}$	20.1	23.4	17.3	20.3 ± 3.1

Table 20. Summary of *Lm*SP-His_6 and *Lm*SP-CL constructs immobilized on Ni-NTA Superflow (approximately 2 mg/mL protein for 10 mg/mL Ni-NTA Superflow)

	Specific activity [U/mg]	Protein loaded [mg]	Activity loaded [U]	Activity in supernatant [U]	Theoretical activity [U]	Theoretical activity [$U/mg_{carrier}$]	Immobilized activity [$U/mg_{carrier}$]	Immobilization Effectiveness [%]
*Lm*SP-His_6	167.0	1.6	267.2	50.1	217.1	21.7	10.0	46.1
*Lm*SP-CL_{5nm}	99.7	2.1	209.4	0	209.4	20.9	23.2	111.0
*Lm*SP-CL_{10m}	106.7	2.0	213.4	0	213.4	21.3	17.3	81.2
*Lm*SP-CL_{15m}	104.1	1.8	187.4	10.4	177.0	17.7	20.3	114.7

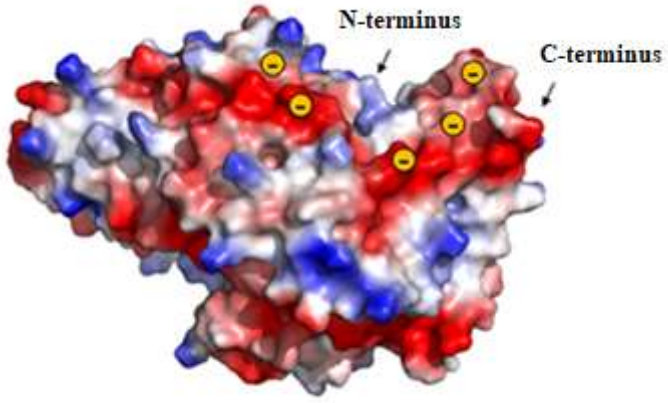

Figure 19. Electrostatic surface analysis of *Lm*SP (UniProt Q59495, AF-Q59495-F1-model_v3.pdb). Negatively charged areas surrounding the N-/C-terminus of the enzyme were marked in red, while the protein parts with positive charges were shown in blue. Electrostatic analysis was performed by using PyMOL (Schrödinger LLC, 2022).

The activity measurement was performed using the discontinuous coupled assay (Chapter 3.2.5.2). As seen in Table 20., the immobilization effectiveness of the *Lm*SP-His_6 was only 46.1 %, which was much lower than that of the *Lm*SP-CL constructs showing values above 80 %. These results further highlight the benefits of linker insertion for enzyme immobilization. As shown in Figure 19, the areas surrounding the N-/C-terminus of *Lm*SP are mainly negatively charged, and these areas would also interact with the positively changed carriers when *Lm*SP is attached to the carriers without a distance or space in between. These unwanted interactions would result in random attachment of enzymes on carriers and possible structural changes of attached enzymes, therefore causing a decrease in activity as compared to the free enzyme (Almeida et al., 2022). In contrast, with a rigid linker in between, the distance between enzymes and carriers increases, and the space surrounding carriers for accommodating enzymes also

increases, the potentially undesired effect from self-interaction of enzymes or interacting with carriers can be minimized (Talbert and Goddard, 2012; Camarero, 2008). The constructs can be assembled on carries in a precise orientation, leading to higher catalytic activity and thus enhanced immobilization effectiveness. Surprisingly, immobilized *Lm*SP-CL_{5nm} and *Lm*SP-CL_{15nm} showed effectiveness above 100%, indicating that the activity of the immobilized enzyme was higher even as compared to the free (solubilized) enzyme. This could have arisen from a measurement error. Also, a possible explanation for that could be as follows: when enzymes are assembled on carriers in high density, the configuration of the enzyme would slightly change, which facilities a further enhanced catalytic process; or the cluster of enzymes would form a boundary layer wherein the substrate is gathered (Rodrigues et al., 2013; Talbert and Goddard, 2012), which would also improve the catalytic process as compared to the free aqueous system. A similar finding was also reported previously. So, Lu et al. (2022) have compared the kinetic parameters of immobilized 4LP-Tpebgl3 (onto Na-Y) and free enzyme. The K_m of the immobilized enzyme was lower (0.37 mM) as compared to the free enzyme (0.58 mM), indicating an improved affinity of the enzyme towards substrate. Also, the k_{cat}/K_m value of the immobilized enzyme was 61 % higher compared to the free enzyme.

Overall, the results in this study suggest that the insertion of a rigid linker [*e.g.* $(EAAAK)_n$] on the C-terminus of *Lm*SP may improve the immobilization yield, also maintaining, and in some cases, improving the activity of the immobilized enzymes as compared to the native enzyme. These advantages, therefore, suggest a potential engineering tool applied for enzyme immobilization.

5. CONCLUSIONS

The conclusions drawn from the results of this study are as follows:

1. Insertion of the rigid α-helix linker [L, $(EAAAK)_n$] with different lengths to N- (NL-*Lm*SP) or C-terminus (*Lm*SP-CL) of *Lm*SP was designed by using POE-PCR, and a series of enzyme constructs were prepared, expressed, purified, and evaluated in terms of enzyme activity.
2. N-terminally fused linkers (NL-*Lm*SP; with the length of 5 and 10 nm) led to undesired performance of two constructs, while C-terminal linker fusion (*Lm*SP-CL; with the length of 5, 10, and 15 nm) retained the properties of *Lm*SP-expression level and enzyme activity. The expression level of N-terminally fused constructs was around 10-fold lower than that of the C-terminally fused constructs (100-150 $mg_{protein}/L_{culture}$). Additionally, lower enzyme activity was observed for the N-terminally fused constructs (~50 U/mg $_{enzyme}$) than for the C-terminally fused constructs (~100 U/mg $_{enzyme}$).
3. Immobilization of the C-terminally fused constructs onto SEPABEADS^{TM} EC-EP suggested that this type of carrier was suitable only for the *Lm*SP constructs with shorter linkers (≤ 10 nm) possibly due to the inhibited spatial diffusion of larger enzyme construct (*Lm*SP-CL_{15nm}).
4. The immobilization of the C-terminally fused constructs (*Lm*SP-CL_{5nm}, *Lm*SP-CL_{10nm}, and *Lm*SP-CL_{15nm}) onto the Ni-NTA Superflow led to a higher immobilization yield (over 90 %, despite the length of linker) when compared to the control (*Lm*SP-His_6), suggesting a potential higher immobilization capacity of *Lm*SP-CL constructs on the carrier.
5. The C-terminally fused constructs showed enhanced immobilization efficiency (*Lm*SP-CL_{5nm}, 111.0 %; *Lm*SP-CL_{10nm}, 81.2 %; *Lm*SP-CL_{15nm}, 114.7 %) as compared to the control (*Lm*SP-His_6; 46.1 %). It might be suggested that the preserved enzyme activity of the C-terminally fused constructs is caused by the templated assembly of the enzyme constructs on the carrier, and it is additionally facilitated by the linkers that may provide more (inter)spaces for enzyme accommodation.

6. LITERATURE

Aggarwal S, Chakravarty A, Ikram S (2021) A comprehensive review on incredible renewable carriers as promising platforms for enzyme immobilization & thereof strategies. *Int J of Biol Macromol* **167**, 962–986. https://doi.org/10.1016/j.ijbiomac.2020.11.052

Almeida FLC, Prata AS, Forte MBS (2022) Enzyme immobilization: what have we learned in the past five years? *Biofuels, Bioprod Biorefin* **16**, 587–608. https://doi.org/10.1002/bbb.2313

Anonymous (2022) pET21b vector [image], available at: <https://www.genscript.com/gsfiles/vector-map/bacteria/pET-21b.pdf?1290382182> (Accessed 25 August 2022).

Berg JM, Tymoczko JL, Stryer L (2013) Stryer Biochemie, 8. Edition, Springer Berlin Heidelberg, Berlin, Heidelberg.

Block H, Maertens B, Spriestersbach A, Brinker N, Kubicek J, Fabis R, et al. (2009) Chapter 27 Immobilized-Metal Affinity Chromatography (IMAC). E: Richard R, Burgess, Murray P. Deutscher. Guide to Protein Purification, 2nd Edition, Volume 463, Academic Press, Cambridge, p. 439–473.

Brady D, Jordaan J (2009) Advances in enzyme immobilisation. *Biotechol Lett* **31**, 1639–1650. https://doi.org/10.1007/s10529-009-0076-4

Çam T, Osman B, Kara A, Demirbel E, Beşirli N, Irez G (2014) Potentiometric, kinetic, and thermodynamic investigations into Cu $^{2+}$ ion binding properties of vinyl imidazole containing IMAC adsorbent. *J Appl Polym Sci* **131**. https://doi.org/10.1002/app.39751

Camarero JA (2008) Recent developments in the site-specific immobilization of proteins onto solid supports. *Biopolymers* **90**, 450–458. https://doi.org/10.1002/bip.20803

Çelem EB, Önal S (2009) Immobilization of phytase on epoxy-activated Sepabead EC-EP for the hydrolysis of soymilk phytate. *J. Mol. Catal. B: Enzym.* **61**, 150–156. https://doi.org/10.1016/j.molcatb.2009.06.001

Çelem EB, Önal S (2022) Sepabeads EC-EP immobilized α-galactosidase: Immobilization, characterization and application in the degradation of raffinose-type oligosaccharides. *Process Biochem* **116**, 136–147. https://doi.org/10.1016/j.procbio.2022.02.020

Cerdobbel A, Desmet T, de Winter K, Maertens J, Soetaert W (2010a) Increasing the thermostability of sucrose phosphorylase by multipoint covalent immobilization. *J Biotechnol* **150**, 125–130. https://doi.org/10.1016/j.jbiotec.2010.07.029

Cerdobbel A, de Winter K, Desmet T, Soetaert W (2010b) Sucrose phosphorylase as cross-

linked enzyme aggregate: Improved thermal stability for industrial applications. *Biotechnol J* **5**, 1192–1197. https://doi.org/10.1002/biot.201000202

Chen X, Zaro JL, Shen W-C (2013) Fusion protein linkers: Property, design and functionality. *Adv Drug Delivery Rev* **65**, 1357–1369. https://doi.org/10.1016/j.addr.2012.09.039

Faruque S, Tong J, Lacmanovic V, Agbonghae C, Minaya D, Czaja K (2019) The Dose Makes the Poison: Sugar and Obesity in the United States – a Review. *Pol J Food Nutr Sci* **69**, 219–233. https://doi.org/10.31883/pjfns/110735

Franceus J, Desmet T (2020) Sucrose Phosphorylase and Related Enzymes in Glycoside Hydrolase Family 13: Discovery, Application and Engineering. *Int J Mol Sci* **21**, 2526. https://doi.org/10.3390/ijms21072526

Garcia-Galan C, Berenguer-Murcia Á, Fernandez-Lafuente R, Rodrigues RC (2011) Potential of Different Enzyme Immobilization Strategies to Improve Enzyme Performance. *Adv Synth Catal* **353**, 2885–2904. https://doi.org/10.1002/adsc.201100534

George RA, Heringa J (2002) An analysis of protein domain linkers: their classification and role in protein folding. *Protein Eng Des Sel* **15**, 871–879. https://doi.org/10.1093/protein/15.11.871

Georgiou G, Valax P (1996) Expression of correctly folded proteins in Escherichia coli. *Curr Opin Biotechnol* **7**, 190–197. https://doi.org/10.1016/S0958-1669(96)80012-7

Goedl C, Sawangwan T, Wildberger P, Nidetzky B (2010) Sucrose phosphorylase: a powerful transglucosylation catalyst for synthesis of α-D-glucosides as industrial fine chemicals. *Biocatal Biotransform* **28**, 10–21. https://doi.org/10.3109/10242420903411595

Goedl C, Schwarz A, Minani A, Nidetzky B (2007) Recombinant sucrose phosphorylase from Leuconostoc mesenteroides: Characterization, kinetic studies of transglucosylation, and application of immobilised enzyme for production of α-d-glucose 1-phosphate. *J Biotechnol* **129**, 77–86. https://doi.org/10.1016/j.jbiotec.2006.11.019

Gonçalves MCP, Kieckbusch TG, Perna RF, Fujimoto JT, Morales SAV, Romanelli JP (2019) Trends on enzyme immobilization researches based on bibliometric analysis. *Process Biochem* **76**, 95–110. https://doi.org/10.1016/j.procbio.2018.09.016

Guzik U, Hupert-Kocurek K, Wojcieszyńska D (2014) Immobilization as a Strategy for Improving Enzyme Properties-Application to Oxidoreductases. *Molecules* **19**, 8995–9018. https://doi.org/10.3390/molecules19078995

Hanefeld U, Gardossi L, Magner E (2009) Understanding enzyme immobilisation. *Chem Soc Rev* **38**, 453–468. https://doi.org/10.1039/B711564B

Hilterhaus L, Minow B, Müller J, Berheide M, Quitmann H, Katzer M, et al. (2008) Practical

application of different enzymes immobilized on sepabeads. *Bioprocess Biosyst Eng* **31**, 163–171. https://doi.org/10.1007/s00449-008-0199-3

Hoai NT, Kim D (2009) Synthesis, structure, and selective separation behavior of copper-imprinted microporous polymethacrylate beads. *AIChE J* **55**, 3248–3254. https://doi.org/10.1002/aic.11943

Homaei AA, Sariri R, Vianello F, Stevanato R (2013) Enzyme immobilization: an update. *J Chem Biol* **6**, 185–205. https://doi.org/10.1007/s12154-013-0102-9

Hsieh H-J, Liu P-C, Liao W-J (2000) Immobilization of invertase via carbohydrate moiety on chitosan to enhance its thermal stability. *Biotechnol Lett* **22**, 1459–1464. https://doi.org/10.1023/A:1005602812037

Knezevic Z, Milosavic N, Bezbradica D, Jakovljevic Z, Prodanovic R (2006) Immobilization of lipase from Candida rugosa on Eupergit® C supports by covalent attachment. *Biochem Eng J* **30**, 269–278. https://doi.org/10.1016/j.bej.2006.05.009

Koga T, Nakamura K, Shirokane Y, Mizusawa K, Kitao S, Kikuchi M (1991) Purification and Some Properties of Sucrose Phosphorylase from *Leuconostoc mesenteroides*. *Agr Biol Chem* **55**, 1805–1810. https://doi.org/10.1080/00021369.1991.10870859

Kurlemann N, Liese A (2004) Immobilization of benzaldehyde lyase and its application as a heterogeneous catalyst in the continuous synthesis of a chiral 2-hydroxy ketone. *Tetrahedron: Asymmetr* **15**, 2955–2958. https://doi.org/10.1016/j.tetasy.2004.07.039

Lu S, Zou K, Guo B, Pei J, Wang Z, Xiao W, et al. (2022) One-step purification and immobilization of thermostable β-glucosidase on Na-Y zeolite based on the linker and its application in the efficient production of baohuoside I from icariin. *Bioorg Chem* **121**, 105690. https://doi.org/10.1016/j.bioorg.2022.105690

Madoery RR, Fidelio GD (2001) A simple method to obtain a covalent immobilized phospholipase A2. *Bioorg Med Chem Lett* **11**, 1663–1664. https://doi.org/10.1016/S0960-894X(01)00277-3

Microsoft Corporation (2010) Microsoft Office Excel (Version 365). https://www.microsoft.com/hr-hr/microsoft-365/excel Accessed from 15th of June 2021.

Mohamad NR, Marzuki NHC, Buang NA, Huyop F, Wahab RA (2015) An overview of technologies for immobilization of enzymes and surface analysis techniques for immobilized enzymes. *Biotechnol Biotec Eq* **29**, 205–220. https://doi.org/10.1080/13102818.2015.1008192

Nguyen HH, Kim M (2017) An Overview of Techniques in Enzyme Immobilization. *Appl Sci Converg Technol* **26**, 157–163. https://doi.org/10.5757/ASCT.2017.26.6.157

Nwagu TN, Aoyagi H, Okolo BN, Yoshida S (2012) Immobilization of a saccharifying raw starch hydrolyzing enzyme on functionalized and non-functionalized sepa beads. *J Mol Catal B: Enzym* **78**, 1–8. https://doi.org/10.1016/j.molcatb.2012.01.019

Olson B, and Markwell J (2007) Assays for Determination of Protein Concentration. *Curr Protoc Pharmacol*, **38**(1). doi:10.1002/0471141755.pha03as38

Passerini A, Punta M, Ceroni A, Rost B, Frasconi P (2006) Identifying cysteines and histidines in transition-metal-binding sites using support vector machines and neural networks. *Proteins: Struct Funct Bioinf* **65**, 305–316. https://doi.org/10.1002/prot.21135

Pimentel MCB, Ferreira MSS (1991) Immobilized sucrose phosphorylase from *Leuconostoc mesenteroides*. *Appl Biochem Biotechnol* **27**, 37–43. https://doi.org/10.1007/BF02921513

Rodrigues RC, Ortiz C, Berenguer-Murcia Á, Torres R, Fernández-Lafuente R (2013) Modifying enzyme activity and selectivity by immobilization. *Chem Soc Rev* **42**, 6290–6307. https://doi.org/10.1039/C2CS35231A

Russell RR, Mukasa H, Shimamura A, Ferretti JJ (1988) Streptococcus mutans gtfA gene specifies sucrose phosphorylase. *Infect Immun* **56**, 2763–2765. https://doi.org/10.1128/iai.56.10.2763-2765.1988

Schmid A, Hollmann F, Park JB, Bühler B (2002) The use of enzymes in the chemical industry in Europe. *Curr Opin Biotechnol* **13**, 359–366. https://doi.org/10.1016/S0958-1669(02)00336-1

Schoemaker HE, Mink D, Wubbolts MG (2003) Dispelling the Myths--Biocatalysis in Industrial Synthesis. *Science* **299**, 1694–1697. https://doi.org/10.1126/science.1079237

Schrödinger, LLC (2022) The PyMOL Molecular Graphics System (Version 2.0). https://pymol.org/2/#page-top Accessed on 18th of July 2022.

Sheldon RA (2007) Enzyme Immobilization: The Quest for Optimum Performance. *Adv Synth Catal* **349**, 1289–1307. https://doi.org/10.1002/adsc.200700082

Simpson RJ (2006) SDS-PAGE of Proteins. *CSH Protocols* **2006**. https://doi.org/10.1101/pdb.prot4313

Singh V, Kaul S, Singla P, Kumar V, Sandhir R, Chung JH, et al. (2018) Xylanase immobilization on magnetite and magnetite core/shell nanocomposites using two different flexible alkyl length organophosphonates: Linker length and shell effect on enzyme catalytic activity. *Int J Biol Macromol* **115**, 590–599. https://doi.org/10.1016/j.ijbiomac.2018.04.097

Sirisha VL, Jain A, Jain A (2016. Chapter Nine - Enzyme Immobilization: An Overview on Methods, Support Material, and Applications of Immobilized Enzymes. E: Kim SK,

Toldrá F. Advances in Food and Nutrition Research, Academic Press, Volume 79, Cambridge, p. 179–211. https://doi.org/10.1016/bs.afnr.2016.07.004

Spasojevic M, Prodanovic O, Pantic N, Popovic N, Belaz AM, Prodanovic R (2020) The Enzyme Immobilization: Carriers and Immobilization methods. *J Eng Process Manag* **11**, 89–105 https://doi.org/10.7251/JEPM1902089S

Sundberg RJ, Bruce Martin R (1973) Interactions of Histidine and Other Imidazole Derivatives with Transition Metal Ions in Chemical and Biological Systems. *Chem Rev* **74,** 471–517.

Talbert JN, Goddard JM (2012) Enzymes on material surfaces. *Colloids Surf B* **93**, 8–19. https://doi.org/10.1016/j.colsurfb.2012.01.003

Tominaga J, Kamiya N, Doi S, Ichinose H, Maruyama T, Goto M (2005) Design of a Specific Peptide Tag that Affords Covalent and Site-Specific Enzyme Immobilization Catalyzed by Microbial Transglutaminase. *Biomacromolecules* **6**, 2299–2304. https://doi.org/10.1021/bm050193o

van den Broek LAM, van Boxtel EL, Kievit RP, Verhoef R, Beldman G, Voragen AGJ (2004) Physico-chemical and transglucosylation properties of recombinant sucrose phosphorylase from Bifidobacterium adolescentis DSM20083. *Appl Microbiol Biotechnol* **65**, 219–227. https://doi.org/10.1007/s00253-003-1534-x

Voora V, Bermúdez S, Larrea C (2020) Global Market Report: Sugar. *International Institute for Sustainable Development (IISD).* http://www.jstor.org/stable/resrep22026

Wang S, Duan L, Jiang L, Liu K, Wang S (2022) Assembly of peptide linker to amino acid dehydrogenase and immobilized with metal–organic framework. *J Chem Technol Biotechnol* **97**, 741–748. https://doi.org/10.1002/jctb.6959

Weimberg R, Doudoroff M (1954) STUDIES WITH THREE BACTERIAL SUCROSE PHOSPHORYLASES. *J Bacteriol* **68**, 381–388. https://doi.org/10.1128/jb.68.3.381-388.1954

Weinhäusel A, Nidetzky B, Rohrbach M, Blauensteiner B, Kulbe KD (1994) A new maltodextrin-phosphorylase from Corynebacterium callunae for the production of glucose-1-phosphate. *Appl Microbiol Biotechnol* **41**, 510–516. https://doi.org/10.1007/BF00178481

Wu X, Fraser K, Zha J, Dordick JS (2018) Flexible Peptide Linkers Enhance the Antimicrobial Activity of Surface-Immobilized Bacteriolytic Enzymes. *ACS Appl Mater Interfaces* **10**, 36746–36756. https://doi.org/10.1021/acsami.8b14411

Xie J, Zhang Y, Simpson B (2022) Food enzymes immobilization: novel carriers, techniques and applications. *Curr Opin Food Sci* **43**, 27–35.

https://doi.org/10.1016/j.cofs.2021.09.004

Xu H, Wei B, Liu X, Huang Y, Zhou W, Liang H (2022) Robust enhancing stability and fructose tolerance of sucrose phosphorylase by immobilization on Ni-NTA functionalized agarose microspheres for the biosynthesis of 2-α-glucosylglycerol. *Biochem Eng J* **180**, 108362. https://doi.org/10.1016/j.bej.2022.108362

Yu C-C, Kuo Y-Y, Liang C-F, Chien W-T, Wu H-T, Chang T-C, et al. (2012) Site-Specific Immobilization of Enzymes on Magnetic Nanoparticles and Their Use in Organic Synthesis. *Bioconjugate Chem* **23**, 714–724. https://doi.org/10.1021/bc200396r

Zhong C, You C, Wei P, Zhang Y-HP (2017) Simple Cloning by Prolonged Overlap Extension-PCR with Application to the Preparation of Large-Size Random Gene Mutagenesis Library in *Escherichia coli*. Hughes, R. Synthetic DNA. Methods in Molecular Biology, vol 1472. Humana Press, New York p 49–61. https://doi.org/10.1007/978-1-4939-6343-0_4

Zucca P, Fernandez-Lafuente R, Sanjust E (2016) Agarose and Its Derivatives as Supports for Enzyme Immobilization. *Molecules* **21**, 1577. https://doi.org/10.3390/molecules21111577

List of abbreviations

16-PHDA	16-phosphonohexadecanoic acid
3-PPA	3-phosphonopropionic acid
AP	Alkaline phosphatase
AU	Absorbance units
BFD	Benzoylformate decarboxylase
BIOTE	The Institute of Biotechnology and Biochemical Engineering
BSA	Bovine serum albumin
*Ca*LB	Lipase B from *Candida antarctica*
CLEA	Cross-linking enzyme aggregate
CLEC	Cross-linking enzyme crystal
CMP	Cytidine monophosphate
CSS	Sialic acid synthetase
ddH_2O	Nano-pure (double distilled) water
dH_2O	Distilled water
dNTP	Deoxynucleotide triphosphate
DTT	Dithiothreitol
EAAAK	Rigid linker sequence of Glutamate, 3× Alanine, and Lysine
EDC	1-ethyl-3-(3-dimethylaminopropyl)-1-carbodiimide hydrochloride
EDTA	Ethylenediaminetetraacetic acid
FAO	Food and Agriculture Organization of the United Nations
G6P-DH	Glucose 6 - phosphate dehydrogenase
GH13	Glycoside hydrolase family 13
Glc-1,6-bP	Glucose 1,6 - bisphosphate
Glc-1-P	Glucose 1-phosphate
HCl	Hydrogen chloride
IF	Insert gene forward primer
IMAC	Immobilized-metal affinity chromatography
IPTG	Isopropyl-β-D-1-thiogalactopyranoside
IR	Insert gene reverse primer

LB medium	Lysogeny Broth medium
LDS	Lithium dodecyl sulfate
*Lm*SP	Sucrose phosphorylase from *Leuconostoc mesenteroides*
*Lm*SP-CL	*Lm*SP with linker on C-terminus
*Lm*SP-CL_{10nm}	*Lm*SP fused with 10 nm linker on C-terminus
*Lm*SP-CL_{15nm}	*Lm*SP fused with 15 nm linker on C-terminus
*Lm*SP-CL_{5nm}	*Lm*SP fused with 5 nm linker on C-terminus
*Lm*SP-His6	C-terminally His-tagged *Lm*SP
Lst	Lysostaphin
MNP	Magnetic nanoparticles
MOPS	3-(N-morpholino)-propane sulphonic acid
NAD^+	Nicotinamide adenine dinucleotide (oxidized form)
NADH	Nicotinamide adenine dinucleotide (reduced form)
NaOH	Sodium hydroxide
NL_{10nm}-*Lm*SP	*Lm*SP fused with 10 nm linker on N-terminus
NL_{5nm}-*Lm*SP	*Lm*SP fused with 5 nm linker on N-terminus
NL-*Lm*SP	*Lm*SP with linker on N-terminus
NTA	Nitrilotriacetic acid
OD	Optical density
OECD	Organization for Economic Co-operation and Development
PCR	Polymerase chain reaction
PG	Polyglutaraldehyde
PGM	Phosphoglucomutase
Pi	Phosphate
PK	Pharmacokinetic
PLA_2	Phospholipase A_2
PmST_1	Sialyltransferase from *Pasteurella multocida*
POE-PCR	Prolonged overlap extension - PCR
RSDA	Raw starch digesting amylase

SDS-PAGE	Sodium dodecyl sulfate - polyacrylamide gel electrophoresis
SEM	Scanning electron microscopy
SP	Sucrose phosphorylase
TAE buffer	Tris-acetate-EDTA buffer
Tpebgl3	Thermostable β-galactosidase
TU Graz	Graz University of Technology
VF	Vector backbone forward primer
VR	Vector backbone reverse primer
ZIF-8	Zeolite imidazolate frameworks-8

STATEMENT OF ORIGINALITY

This is to certify, that the intellectual content of this thesis is the product of my own independent and original work and that all the sources used in preparing this thesis have been duly acknowledged.

Ivan Mikac